

**University of Stuttgart**  
Germany



## BACHELOR'S THESIS

# A Multi-grid method

on the Cahn-Hilliard equation and its relaxed variation.

Jonathan Ulmer

Matriculation Number: 3545737

Supervisor: Prof. Dr. Christian Rohde

Institute of Applied Analysis and Numerical Simulation

Completed 21.08.2024



## **Abstract**

This Thesis gives a short overview and derivation for the Cahn-Hilliard Equation. It uses a discretization by the authors [1] as baseline, and expands upon this discretisation with an elliptical relaxation approach. It introduces evaluation metrics regarding stability in time, space and during sub-iteration. And compares the elliptical approach against the baseline. Furthermore, it shows a qualitative success of the elliptical solver, however it also highlights challenges in numerical stability.



# CONTENTS

1	INTRODUCTION	1
2	THE CAHN-HILLIARD EQUATION	3
2.1	Physical derivation of the CH equation (2.1) . . . . .	3
2.1.1	The free energy . . . . .	3
2.1.2	Derivation of the CH equation from mass balance . . . . .	4
2.2	initial value problem . . . . .	6
3	DISCRETIZATION OF THE CH EQUATION	7
3.1	The discretization of functions and derrivative operators . . . . .	7
3.2	Initial data . . . . .	10
3.3	Discretization into a linear system . . . . .	12
4	NUMERICAL SOLVER	15
4.1	Gauss-Seidel smoothing . . . . .	15
4.2	Two-grid method . . . . .	16
4.2.1	Pre Smoothing . . . . .	17
4.2.2	Restriction . . . . .	17
4.2.3	Course grid solution . . . . .	17
4.2.4	Prolongation . . . . .	17
4.2.5	Post Smoothing . . . . .	18
4.2.6	additional considerations . . . . .	18
5	NUMERICAL EXPERIMENTS	21
5.1	Energy evaluations . . . . .	21
5.2	Numerical mass conservation . . . . .	22
5.3	Stability of a two-grid sub-iteration . . . . .	24
5.4	Stability in time . . . . .	25
5.5	Stability in space . . . . .	26

<b>6 RELAXED CAHN-HILLIARD EQUATION</b>	29
6.1 Relaxed energy functional . . . . .	29
6.2 Relaxed mass conservation . . . . .	30
6.3 Relaxed initial value problem . . . . .	30
<b>7 DISCRETIZATION OF THE RELAXED PROBLEM</b>	31
7.1 Elliptical PDE . . . . .	31
7.2 Gauss Seidel solver for the elliptical system . . . . .	32
7.3 Relaxed system . . . . .	33
7.4 Relaxed Gauss-Seidel iteration . . . . .	34
7.5 The relaxed multigrid method . . . . .	36
<b>8 DISCRETE MASS CONSERVATION</b>	39
<b>9 RELAXED EXPERIMENTS</b>	43
9.1 Relaxed energy evaluations . . . . .	43
9.2 Stability of a relaxed multigrid sub-iteration . . . . .	44
9.3 Relaxed numerical mass balance . . . . .	45
9.4 Relaxed stability in time . . . . .	46
9.5 Relaxed stability in space . . . . .	47
<b>10 COMPARISON</b>	49
10.1 effect of alpha . . . . .	49
10.2 Direct comparison . . . . .	50
10.3 optimizer for alpha . . . . .	51
<b>11 CONCLUSION</b>	53
11.1 Outlook . . . . .	53
<b>12 APPENDIX</b>	55
12.1 Operator implementation . . . . .	55
12.1.1 relaxed . . . . .	55
12.2 rng generation . . . . .	55
12.3 alternative experiments . . . . .	56
12.3.1 iteration . . . . .	56
12.3.2 subiteration . . . . .	58
12.4 alternative results . . . . .	61
12.4.1 iteration . . . . .	61

12.4.2 subiteration . . . . .	61
12.4.3 mass . . . . .	61
12.5 Monte Carlo optimizer . . . . .	62
12.6 bulk energy and mass balance . . . . .	64



# 1 INTRODUCTION

The Cahn-Hilliard (CH) equation is a well known fourth order partial differential equation (PDE) used in multi-phase flow. It is used to couple different phases with a diffuse-interface. It does this using a continuous transition between two phases. The CH equation, being fourth order, is difficult to solve numerically. However it is still used since it is able to guarantee conservation of mass. In this thesis we implement numerical solvers for the Cahn-Hilliard equation in the Julia programming language. We begin by giving an overview and a derivation for the analytical CH equation in Chapter 2. We then show mass conservation and a decrease of total energy in time. The Chapter 3 introduces our finite difference discretization. We explain the necessary functions, and give their implementation. Additionally we introduce the initial conditions we used in this thesis. Chapter 4 describes the relevant steps of our numerical implementation in the two-grid method we used. In Chapter 5 we evaluate this method's stability, discrete mass conservation and discrete energy decrease that we have shown continuously for the analytical CH equation. Our thesis introduces a elliptical relaxation approach to the classical CH equation, where instead of solving a fourth order PDE <sup>1</sup>, we solve a second order relaxed PDE and an additional elliptical PDE. In the chapter 6 we introduce this approach, and then derive a numerical solver using the method described in chapter 4.2. Hereupon we derive and implement the necessary functions for the discretized relaxed equation, and we introduce a simple solver for the elliptical PDE. Subsequently, in chapter 9, we evaluate our relaxed method against the baseline with the same measures, as introduced in chapter 5.

We began writing this thesis with a reproducible research philosophy in mind. Hence, we provide the explanation and the implementation in the same file. The original aim was to have the mathematical formulas and their implementation interleaved. While we fall short of this goal, we still provide all relevant code in the relevant sections and the appendix. All shown code is therefore the code that

---

<sup>1</sup>This solver uses a two dimensional version with 2 second order terms instead of the full fourth order equation.

## *1 Introduction*

is run on our machine. Since not all parts of the code are relevant for understanding, unimportant sections are implemented elsewhere. Didactically they are replaced with a comment of form <<unimportant-code-section>>. Their implementation can be found in `Thesis_jl.org` in a code block of the same name. We did experiment with additional tools such as `org-mode` that allow for scientific note-taking and literate programming. This file is available on our github repository at <https://github.com/ProceduralTree/CahnHilliardJulia.git> as `Thesis_jl.org`. The code to our numerical experiments we provide in the appendix as well as under `experiments/src/` in the repository. We provide the code for the plots next to them in `Thesis_jl.org`. The code for the numerical solvers themselves is in both the PDF and the ORG Document, and gets exported into the `src/` directory of the github repository.

# 2 THE CAHN-HILLIARD EQUATION

The Cahn-Hilliard (CH) equation is a partial differential equation (PDE) that governs the dynamics of a two-phase fluid [2]. The form of the CH equation used in this thesis in the domain  $\Omega \times (0, T)$ ,  $\Omega \subset \mathbb{R}^d$ ,  $d \in \mathbb{N}$ ,  $T > 0$ ,

$$\begin{aligned}\partial_t \phi(x, t) &= \nabla \cdot (M(\phi) \nabla \mu), \\ \mu &= -\varepsilon^2 \Delta \phi + W'(\phi),\end{aligned}\tag{2.1}$$

where respectively, the variables  $\phi, \mu : \Omega \times (0, T) \rightarrow \mathbb{R}^d$  are phase-field variable and chemical potential,  $\varepsilon$  is a positive constant correlated with interface thickness,  $W(\phi)$  is a double well potential and  $M(\phi) > 0$  is a mobility coefficient [2].  $\phi$  is defined in an interval  $I = [-1, 1]$  and represent the different phases.

$$\phi = \begin{cases} 1 & , \phi \in \text{phase 1} \\ -1 & , \phi \in \text{phase 2} \end{cases}$$

In this thesis we assume  $M(\phi) \equiv 1$ , simplifying the CH equation.

The advantages of the CH approach, as compared to traditional boundary coupling, are for example: “explicit tracking of the interface” [2], as well as “evolution of complex geometries and topological changes [...] in a natural way” [2]. In practice, it enables linear interpolation between different formulas on different phases.

## 2.1 PHYSICAL DERIVATION OF THE CH EQUATION (2.1)

### 2.1.1 THE FREE ENERGY

The authors in [2] define the CH equation using the **Ginzburg-Landau** free energy equation:

$$E^{\text{bulk}}[\phi] = \int_{\Omega} \frac{\varepsilon^2}{2} |\nabla \phi|^2 + W(\phi) dx,\tag{2.2}$$

## 2 The Cahn-Hilliard equation

where  $W(\phi)$  denotes the Helmholtz free energy density of mixing [2] that we approximate it in further calculations with  $W(\phi) = \frac{(1-\phi^2)^2}{4}$  as in [1] shown in Fig. 2.1.

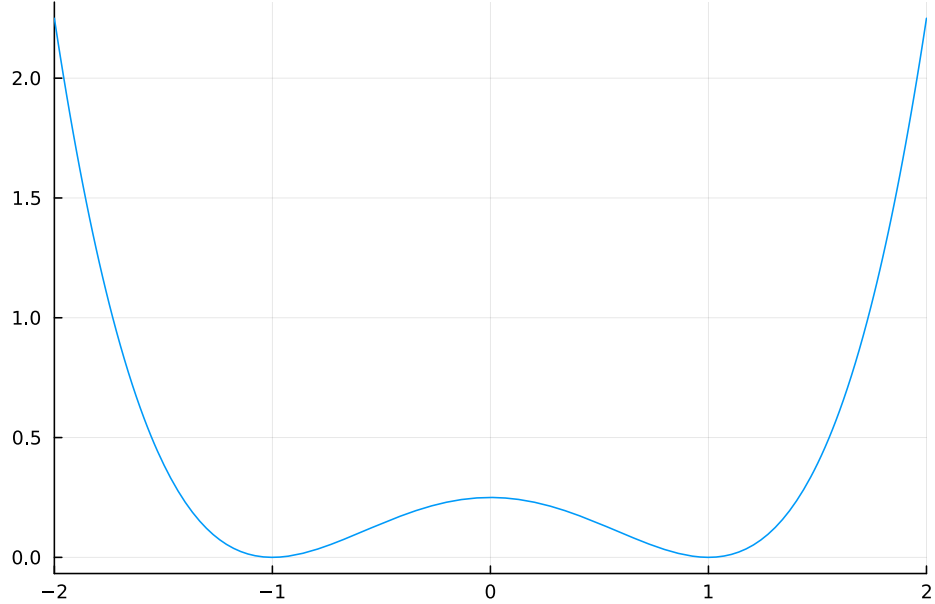


Figure 2.1: Double well potential  $W(\phi)$

The chemical potential,  $\mu$ , then follows as the variational derivation of the free energy in (2.2).

$$\mu = \frac{\delta E_{bulk}(\phi)}{\delta \phi} = -\varepsilon^2 \Delta \phi + W'(\phi) \quad (2.3)$$

### 2.1.2 DERIVATION OF THE CH EQUATION FROM MASS BALANCE

The paper [2] states that the observable phase separation is driven by a diffusion resulting from the gradient in chemical potential  $\mu$ . The emergent conservative dynamics motivate the following diffusion equation

$$\partial_t \phi + \nabla \cdot \mathbf{J} = 0, \quad (2.4)$$

## 2.1 Physical derivation of the CH equation (2.1)

where  $\mathbf{J} = -\nabla\mu$  represents mass-flux. We follow the authors [2] in deriving the CH equation by combining (2.3) and (2.4).

$$\begin{aligned} \implies \partial_t\phi &= -\nabla \cdot \mathbf{J} = \Delta\mu, \\ \mu &= -\varepsilon^2\Delta\phi + W'(\phi), \end{aligned} \tag{2.5}$$

Furthermore the CH equation is mass conservative under homogeneous Neumann boundary conditions, defined as:

$$\begin{aligned} \mathbf{J} \cdot \mathbf{n} &= 0 \quad \text{on } \partial\Omega \times (0, T), \\ \partial_n\phi &= 0 \quad \text{on } \partial\Omega \times (0, T), \end{aligned} \tag{2.6}$$

where  $\mathbf{n}$  is the outward normal on  $\partial\Omega$ . To show the conservation of mass we analyze the change in total mass in the domain  $\Omega$  over time.

$$\begin{aligned} \frac{d}{dt} \int_{\Omega} \phi \, d\mathbf{x} &= \int_{\Omega} \frac{\partial\phi}{\partial t} \, d\mathbf{x} \\ &= - \int_{\Omega} \nabla \cdot \mathbf{J} \, d\mathbf{x} \\ &= \int_{\partial\Omega} \mathbf{J} \cdot \mathbf{n} \, ds \\ &= 0 \quad \forall t \in (0, T), \end{aligned} \tag{2.7}$$

In order to show thermodynamic consistency of the CH equation, we take the time derivation of the free energy functional (2.2).

$$\begin{aligned} \frac{d}{dt} E^{bulk}[\phi(t)] &= \int_{\Omega} (\varepsilon^2 \nabla\phi \cdot \nabla\partial_t\phi + W'(\phi)\partial_t\phi) \, d\mathbf{x} \\ &= \int_{\Omega} (\varepsilon^2 \nabla\phi + W'(\phi))\partial_t\phi \, d\mathbf{x} \\ &= \int_{\Omega} \mu\partial_t\phi \, d\mathbf{x} \\ &= \int_{\Omega} \mu \cdot \Delta\mu \, d\mathbf{x} \\ &= - \int_{\Omega} \nabla\mu \cdot \nabla\mu \, d\mathbf{x} + \int_{\partial\Omega} \mu \nabla\phi_t \cdot \mathbf{n} \, dS \\ &\stackrel{\partial_n\phi=0}{=} - \int_{\Omega} |\nabla\mu|^2 \, d\mathbf{x}, \quad \forall t \in (0, T) \end{aligned}$$

This a bounded  $L_2$  norm on of  $\nabla\mu$ .

## 2 The Cahn-Hilliard equation

### 2.2 INITIAL VALUE PROBLEM

Our Thesis then concerns it self with the initial value problem on the domain  $\Omega \subset \mathbb{R}^2$

$$\begin{aligned}
\partial_t \phi(x, t) &= \nabla \cdot (M(\phi) \nabla \mu), \text{ in } \Omega \times (0, T), \\
\mu &= -\varepsilon^2 \Delta \phi + W'(\phi), \text{ in } \Omega \times (0, T), \\
-\nabla \mu \cdot \mathbf{n} &= 0 \quad \text{on } \partial \Omega \times (0, T), \\
\nabla \phi \cdot \mathbf{n} &= 0 \quad \text{on } \partial \Omega \times (0, T), \\
\phi(x, 0) &= \phi^0(x),
\end{aligned} \tag{2.8}$$

# 3 DISCRETIZATION OF THE CH EQUATION

This thesis used a finite difference discretization of the CH equation in space and time , that is implicit in time.

## 3.1 THE DISCRETIZATION OF FUNCTIONS AND DERRIVATIVE OPERATORS

As baseline for numerical experiments we use a two-grid method based on the finite difference method defined in [1]. Our discretization follows the one taken by the authors in [1]. We discretize our domain  $\Omega$  to be a Cartesian-grid  $\Omega_d$  on a square with side-length  $N \cdot h$ , where  $N$  is the number of grid-points in one direction, and  $h$  is the distance between grid-points. In all our initial data  $h$  is  $3 \cdot 10^{-3}$  and  $N = 64$ . However, for stability tests we change  $h$  and  $N$ . The discrete version or our domain is

$$\Omega_d = \{i, j \mid i, j \in \mathbb{N}, i, j \in [2, N + 1]\}, \quad (3.1)$$

as shown in 3.1

### 3 Discretization of the CH equation

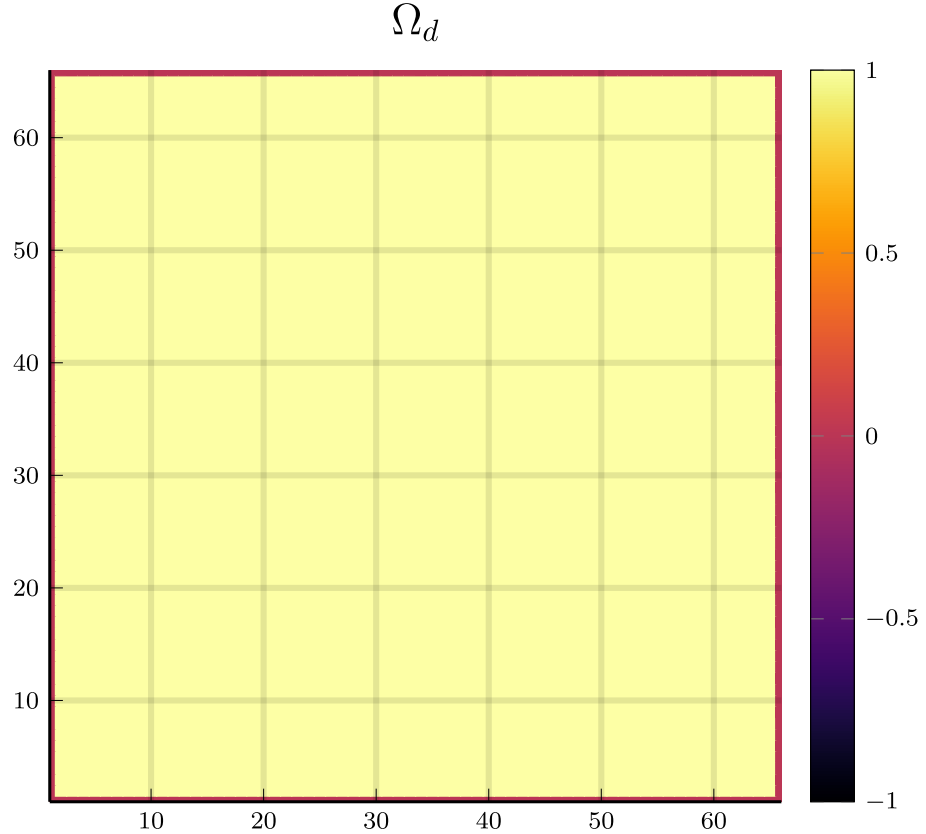


Figure 3.1: Discrete Domain used in this Thesis. 1 is inside and 0 outside of the Domain.

We discretize the phase-field  $\phi$ , and chemical potential  $\mu$ , into grid-wise functions  $\phi_{ij}, \mu_{ij}$  such that

$$\begin{aligned}\phi_{ij}^n : \Omega_d \times \{0, \dots\} &\rightarrow \mathbb{R}, \\ \mu_{ij}^n : \Omega_d \times \{0, \dots\} &\rightarrow \mathbb{R},\end{aligned}\tag{3.2}$$

Here  $n$  denotes the  $n$ th time-step, and  $(i, j)$  are Cartesian indices on the discrete domain  $\Omega_d$ . The authors in [1] then use the characteristic function  $G$  of the domain  $\Omega$  to enforce no-flux boundary conditions (2.6).

$$G(x, y) = \begin{cases} 1, & (x, y) \in \Omega \\ 0, & (x, y) \notin \Omega \end{cases}$$

### 3.1 The discretization of functions and derivative operators

We implement the discrete version of  $G$  on  $\Omega_d$  as follows:

$$G_{ij} = \begin{cases} 1, & i, j \in [2, N+1] \\ 0, & \text{else} \end{cases}$$

The definition of  $G_{ij}$  with  $i, j \in [2, N+1]$  enables us to evaluate  $G_{ij}$  off-grid.

```
function G(i, j, len, width)
    if 2 <= i <= len + 1 && 2 <= j <= width + 1
        return 1.0
    else
        return 0.0
    end
end
```

We then define the discrete derivatives  $D_x\phi_{ij}$ ,  $D_y\phi_{ij}$  using finite differences:

$$D_x\phi_{i+\frac{1}{2}j}^{n+1,m} = \frac{\phi_{i+1,j}^{n+1,m} - \phi_{ij}^{n+1,m}}{h} \quad D_y\phi_{ij+\frac{1}{2}}^{n+1,m} = \frac{\phi_{ij+1}^{n+1,m} - \phi_{ij}^{n+1,m}}{h} \quad (3.3)$$

We define  $D_x\mu_{ij}^{n+\frac{1}{2},m}$ ,  $D_y\mu_{ij}^{n+\frac{1}{2},m}$  in the same way. Next we define the discrete gradient  $\nabla_d\phi_{ij}^{n+1,m}$ , as well as a modified Laplacian  $\nabla_d \cdot (G_{ij}\nabla_d\phi_{ij}^{n+1,m})$ :

$$\begin{aligned} \nabla_d\phi_{ij}^{n+1,m} &= \left( D_x\phi_{i+1,j}^{n+1,m}, D_y\phi_{ij+1}^{n+1,m} \right), \\ \nabla_d \cdot (G_{ij}\nabla_d\phi_{ij}^{n+1,m}) &= \frac{G_{i+\frac{1}{2}j}D_x\phi_{i+\frac{1}{2}j}^{n+1,m} - G_{i-\frac{1}{2}}D_x\phi_{i-\frac{1}{2}j}^{n+1,m} + D_y\phi_{ij+\frac{1}{2}}^{n+1,m} - D_y\phi_{ij-\frac{1}{2}}^{n+1,m}}{h} \\ &= \frac{G_{i+\frac{1}{2}j}\phi_{i+1,j}^{n+1,m} + G_{i-\frac{1}{2}}\phi_{i-1,j}^{n+1,m} + G_{ij+\frac{1}{2}}\phi_{ij+1}^{n+1,m} + G_{ij-\frac{1}{2}}\phi_{ij-1}^{n+1,m}}{h^2} \\ &\quad - \frac{\left( G_{i+\frac{1}{2}j} + G_{i-\frac{1}{2}} + G_{ij+\frac{1}{2}} + G_{ij-\frac{1}{2}} \right) \cdot \phi_{ij}^{n+1,m}}{h^2}, \end{aligned} \quad (3.4)$$

The discretization for  $\nabla_d\mu_{ij}^{n+\frac{1}{2},m}$ ,  $\nabla_d \cdot (G_{ij}\nabla_d\mu_{ij}^{n+\frac{1}{2},m})$  are done the same as for  $\phi_{ij}^{n+1}$ . We define  $\nabla_d \cdot (G_{ij}\nabla_d\phi_{ij})$  instead of a discrete Laplacian  $\Delta_d$  to ensure a discrete version of boundary conditions (2.6). The authors in [1] show this to be the case by expanding  $\nabla_d \cdot (G_{ij}\nabla_d\phi_{ij})$ . Notably, when one point lies outside the domain, e.g.  $G_{i+\frac{1}{2}} = 0$  then the corresponding discrete gradient  $\frac{\phi_{i+1}^{n+1} - \phi_i}{h}$  is weighted by 0. This corresponds the discrete version of  $\partial_n\phi = 0$  [1].

### 3 Discretization of the CH equation

To simplify the notation for discretized derivatives we use the following abbreviations:

- $\Sigma_G \phi_{ij} = G_{i+\frac{1}{2}j} \phi_{i+1j}^{n+1,m} + G_{i-\frac{1}{2}j} \phi_{i-1j}^{n+1,m} + G_{ij+\frac{1}{2}} \phi_{ij+1}^{n+1,m} + G_{ij-\frac{1}{2}} \phi_{ij-1}^{n+1,m}$
- $\Sigma_{Gij} = G_{i+\frac{1}{2}j} + G_{i-\frac{1}{2}j} + G_{ij+\frac{1}{2}} + G_{ij-\frac{1}{2}}$

The Code for those abbreviations is:

```

function neighbours_in_domain(i, j, G, len, width)
(
    G(i + 0.5, j, len, width)
    + G(i - 0.5, j, len, width)
    + G(i, j + 0.5, len, width)
    + G(i, j - 0.5, len, width)
)

end

function discrete_G_weighted_neighbour_sum(i, j, arr, G, len, width)
(
    G(i + 0.5, j, len, width) * arr[i+1, j]
    + G(i - 0.5, j, len, width) * arr[i-1, j]
    + G(i, j + 0.5, len, width) * arr[i, j+1]
    + G(i, j - 0.5, len, width) * arr[i, j-1]
)
end

```

We can then write the modified Laplacian  $\nabla_d \cdot (G \nabla_d \phi_{ij}^{n+1})$  as:

$$\nabla_d \cdot (G \nabla_d \phi_{ij}^{n+1}) = \frac{\Sigma_G \phi_{ij}^{n+1} - \Sigma_{Gij} \cdot \phi_{ij}^{n+1}}{h^2} \quad (3.5)$$

We use this modified Laplacian to deal with boundary conditions. Our abbreviations simplify separating implicit and explicit terms in the discretization.

## 3.2 INITIAL DATA

For testing of our numerical solver for (2.8) we use initial discrete phase-fields defined by the following equations:

$$\begin{aligned}
 \phi_{ij}^0 &= \begin{cases} 1 & , \|(i,j) - (\frac{N}{2}, \frac{N}{2})\|_p < \frac{N}{3} \\ -1 & , \text{else} \end{cases} \quad \text{where } p \in \{2, \infty\} \\
 \phi_{ij}^0 &= \begin{cases} 1 & , i < \frac{N}{2} \\ -1 & , \text{else} \end{cases} \\
 \phi_{ij}^0 &= \begin{cases} 1 & , \|(i,j) - (\frac{N}{2}, 2)\|_2 < \frac{N}{3} \\ -1 & , \text{else} \end{cases} \\
 \phi_{ij}^0 &= \begin{cases} 1 & , \|(i,j) - q_k\|_p < \frac{N}{5} \\ -1 & , \text{else} \end{cases} \quad p \in \{1, 2, \infty\}, q_k \in Q
 \end{aligned} \tag{3.6}$$

where  $q_k$  are random points inside my domain. We generate those using the following RNG setup in Julia

```

using Random
rng = MersenneTwister(42)
gridsize = 64
radius = gridsize /5
blobs = gridsize ÷ 5
rngpoints = rand(rng, 1:gridsize, 2, blobs)

```

```

MersenneTwister(42)
64
12.8
12
2×12 Matrix{Int64}:
48  40  20   1  63  49   8  60  26  58  26  11
17  13  56  52  15   9  30  14  40   9  40  25

```

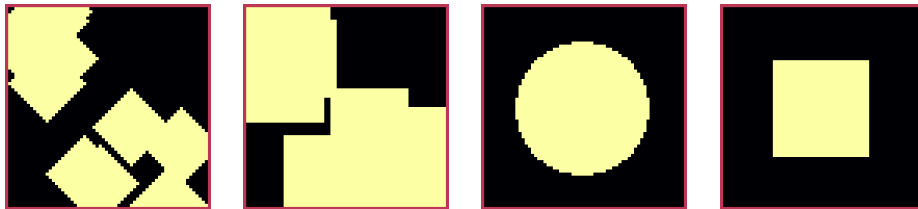


Figure 3.2: Examples of different phase-fields used as the initial condition.

### 3 Discretization of the CH equation

#### 3.3 DISCRETIZATION INTO A LINEAR SYSTEM

The authors in [1] then define the discrete CH equation adapted for the domain as:

$$\begin{aligned} \frac{\phi_{ij}^{n+1} - \phi_{ij}^n}{\Delta t} &= \nabla_d \cdot (G_{ij} \nabla_d \mu_{ij}^{n+\frac{1}{2}}), \\ \mu_{ij}^{n+\frac{1}{2}} &= 2\phi_{ij}^{n+1} - \varepsilon^2 \nabla_d \cdot (G_{ij} \nabla_d \phi_{ij}^{n+1}) + W'(\phi_{ij}^n) - 2\phi_{ij}^n, \end{aligned} \quad (3.7)$$

and derive a numerical scheme from this equation. This method is semi-implicit in time, and consists of a centered difference in space. The authors in [1] derive their method by separating (3.7) into implicit and linear terms, and explicit non-linear terms. We write the implicit terms in form of a function  $L : \mathbb{R}^2 \rightarrow \mathbb{R}^2$  and the explicit terms in  $(\zeta_{ij}^n, \psi_{ij}^n)^T$ . We define  $L$  as:

$$L \begin{pmatrix} \phi_{ij}^{n+1} \\ \mu_{ij}^{n+\frac{1}{2}} \end{pmatrix} := \begin{pmatrix} \frac{\phi_{ij}^{n+1}}{\Delta t} - \nabla_d \cdot (G_{ij} \nabla_d \mu_{ij}^{n+\frac{1}{2}}) \\ \varepsilon^2 \nabla_d \cdot (G \nabla_d \phi_{ij}^{n+1}) - 2\phi_{ij}^{n+1} + \mu_{ij}^{n+\frac{1}{2}} \end{pmatrix}.$$

```
function L(solver::multi_solver,i,j , phi , mu)
    xi = solver.phase[i, j] / solver.dt -
        (discrete_G_weighted_neigbour_sum(i, j, solver.potential, G, solver.len,
        ↪ solver.width) -
        -
        neighbours_in_domain(i, j, G, solver.len, solver.width) * mu
        ↪ )/solver.h^2
    psi = solver.epsilon^2/solver.h^2 *
        (discrete_G_weighted_neigbour_sum(i, j, solver.phase, G, solver.len,
        ↪ solver.width) -
        -
        neighbours_in_domain(i, j, G, solver.len, solver.width) * phi) - 2 *
        ↪ phi + mu
    return [xi, psi]
end
```

This function follows from (3.7) and is linear in the unknowns  $\left(\phi_{ij}^{n+1}, \mu_{ij}^{n+\frac{1}{2}}\right)$ . The non-linear terms of (3.7) are collected in  $\left(\zeta_{ij}^n, \psi_{ij}^n\right)$ . Which we define as

$$\begin{pmatrix} \zeta_{ij}^n \\ \psi_{ij}^n \end{pmatrix} := \begin{pmatrix} \frac{\phi_{ij}^n}{\Delta t} \\ W'(\phi_{ij}^n) - 2\phi_{ij}^n \end{pmatrix}.$$

```

function set_xi_and_psi!(solver::T) where T <: Union{multi_solver ,
    ↪ relaxed_multi_solver}
    xi_init(x) = x / solver.dt
    psi_init(x) = solver.W_prime(x) - 2 * x
    solver.xi[2:end-1, 2:end-1] = xi_init.(solver.phase[2:end-1, 2:end-1])
    solver.psi[2:end-1, 2:end-1] = psi_init.(solver.phase[2:end-1, 2:end-1])
    return nothing
end

```

The authors [1] defined a numerical method where all non linear terms are evaluated explicitly. Therefore , we know everything needed to calculate  $(\zeta_{ij}^n, \psi_{ij}^n)^T$  at the beginning of each time step. We compute those values once and store them in the solver. Using  $(\zeta_{ij}^n, \psi_{ij}^n)$  and  $L\left(\phi_{ij}^{n+1}, \mu_{ij}^{n+\frac{1}{2}}\right)$  , we can rewrite (3.7) as

$$L\begin{pmatrix} \phi_{ij}^{n+1} \\ \mu_{ij}^{n+\frac{1}{2}} \end{pmatrix} = \begin{pmatrix} \zeta_{ij}^n \\ \psi_{ij}^n \end{pmatrix}. \quad i, j \in \{1, \dots, N\} \quad (3.8)$$

This Linear system consists of NxN, 2 dimensional linear equations. Each equation in the linear system (3.8) can be rewritten in the form  $\mathbf{DL}_{ij} \cdot \begin{pmatrix} \phi_{ij}^{n+1}, \mu_{ij}^{n+\frac{1}{2}} \end{pmatrix}^T = b_{ij}$ : Where  $\mathbf{DL}_{ij}$  is

$$\mathbf{DL}_{ij} = \begin{pmatrix} \frac{1}{\Delta t} & \frac{1}{h^2} \Sigma_{Gij} \\ -\frac{\varepsilon^2}{h^2} \Sigma_{Gij} - 2 & 1 \end{pmatrix}$$

and where  $\Sigma_{Gij} = G_{i+\frac{1}{2}j} + G_{i-\frac{1}{2}j} + G_{ij+\frac{1}{2}} + G_{ij-\frac{1}{2}}$

```

function dL(solver::multi_solver , i , j)
    return [ (1/solver.dt) (1/solver.h^2*neighbours_in_domain(i,j,G,solver.len ,
    ↪ solver.width));
        ↪ (-1*solver.epsilon^2/solver.h^2 *
        ↪ neighbours_in_domain(i,j,G,solver.len , solver.width) - 2) 1]
end

```

$\mathbf{DL}_{ij}$  is invertible, since its determinant is positive. Therefore the system (3.8) is solvable

$$\det(\mathbf{DL}_{ij}) = \frac{1}{\Delta t} + \frac{1}{h^2} \Sigma_{Gij} \left( + \frac{\varepsilon^2}{h^2} \Sigma_{Gij} + 2 \right) > 0 \quad (3.9)$$

### 3 Discretization of the CH equation

as  $\Sigma_{Gij} \in \{0, 1, 2, 3, 4\}$ . Using The abbreviation for  $\nabla_d \cdot (G_{ij} \nabla_d \mu_{ij}^{n+\frac{1}{2}})$  introduced in (3.5) , and we rewrite (3.8) in terms of  $\mathbf{DL}_{ij}$

$$\begin{aligned} L \begin{pmatrix} \phi_{ij}^{n+1} \\ \mu_{ij}^{n+\frac{1}{2}} \end{pmatrix} &= \begin{pmatrix} \zeta_{ij}^n \\ \psi_{ij}^n \end{pmatrix} \\ \implies \mathbf{DL}_{ij} \cdot \begin{pmatrix} \phi_{ij}^{n+1} \\ \mu_{ij}^{n+\frac{1}{2}} \end{pmatrix} + \begin{pmatrix} -\frac{1}{h^2} \Sigma_{Gij} \mu_{ij}^{n+\frac{1}{2}} \\ + \frac{\varepsilon^2}{h^2} \Sigma_{Gij} \phi_{ij}^{n+1} \end{pmatrix} &= \begin{pmatrix} \zeta_{ij}^n \\ \psi_{ij}^n \end{pmatrix}, \\ \implies \mathbf{DL}_{ij} \cdot \begin{pmatrix} \phi_{ij}^{n+1} \\ \mu_{ij}^{n+\frac{1}{2}} \end{pmatrix} &= \begin{pmatrix} \zeta_{ij}^n \\ \psi_{ij}^n \end{pmatrix} - \begin{pmatrix} -\frac{1}{h^2} \Sigma_{Gij} \mu_{ij}^{n+\frac{1}{2}} \\ + \frac{\varepsilon^2}{h^2} \Sigma_{Gij} \phi_{ij}^{n+1} \end{pmatrix}, \end{aligned} \quad (3.10)$$

where

- $\Sigma_G \phi_{ij}^{n+1} = G_{i+\frac{1}{2}j} \phi_{i+1j}^{n+1,m} + G_{i-\frac{1}{2}j} \phi_{i-1j}^{n+1,m} + G_{ij+\frac{1}{2}} \phi_{ij+1}^{n+1,m} + G_{ij-\frac{1}{2}} \phi_{ij-1}^{n+1,m}$ ,  $\Sigma_G \mu_{ij}^{n+\frac{1}{2}} = G_{i+\frac{1}{2}j} \mu_{i+1j}^{n+\frac{1}{2},m} + G_{i-\frac{1}{2}j} \mu_{i-1j}^{n+\frac{1}{2},m} + G_{ij+\frac{1}{2}} \mu_{ij+1}^{n+\frac{1}{2},m} + G_{ij-\frac{1}{2}} \mu_{ij-1}^{n+\frac{1}{2},m}$ ,

# 4 NUMERICAL SOLVER

The multi-grid method consists of a linear Gauss-Seidel solver, restriction and prolongation methods, to move course and fine grids.

## 4.1 GAUSS-SEIDEL SMOOTHING

The authors [1] derived Gauss-Seidel Smoothing from (3.8) : Smoothing denoted as a SMOOTH operator consists of a Gauss-Seidel method, by solving (3.10) for all  $i, j$  with the initial guess for  $\zeta_{ij}^n, \psi_{ij}^n$ . We define an iterative Gaus Seidel method. After having solved equation (3.8) for  $(i - 1, j), (i, j - 1)$  we define the Gaus-Seidel iteration in  $s$  for  $(i, j)$  as follows:

$$\mathbf{DL}_{ij} \cdot \begin{pmatrix} \phi_{ij}^{n+1,s+1} \\ \mu_{ij}^{n+\frac{1}{2},s+1} \end{pmatrix} = \begin{pmatrix} \zeta_{ij}^n \\ \psi_{ij}^n \end{pmatrix} - \begin{pmatrix} -\frac{1}{h^2} \Sigma_{Gij} \mu_{ij}^{n+\frac{1}{2},s+\frac{1}{2}} \\ +\frac{\varepsilon^2}{h^2} \Sigma_{Gij} \phi_{ij}^{n+1,s+\frac{1}{2}} \end{pmatrix}, \quad (4.1)$$

where

- $\Sigma_G \phi_{ij}^{n+1,s+\frac{1}{2}} = G_{i+\frac{1}{2}j} \phi_{i+1j}^{n+1,s} + G_{i-\frac{1}{2}j} \phi_{i-1j}^{n+1,s+1} + G_{ij+\frac{1}{2}} \phi_{ij+1}^{n+1,s} + G_{ij-\frac{1}{2}} \phi_{ij-1}^{n+1,s+1}$ ,
- $\Sigma_G \mu_{ij}^{n+\frac{1}{2},s+\frac{1}{2}} = G_{i+\frac{1}{2}j} \mu_{i+1j}^{n+\frac{1}{2},s} + G_{i-\frac{1}{2}j} \mu_{i-1j}^{n+\frac{1}{2},s+1} + G_{ij+\frac{1}{2}} \mu_{ij+1}^{n+\frac{1}{2},s} + G_{ij-\frac{1}{2}} \mu_{ij-1}^{n+\frac{1}{2},s+1}$ ,

This constitutes a Gaus-Seidel method in its element based formula.

```
function SMOOTH!(
    solver::T,
    iterations,
    adaptive
) where T <: Union{multi_solver, adapted_multi_solver, gradient_boundary_solver}
    for s = 1:iterations
        # old_phase = copy(solver.phase)
        for I in CartesianIndices(solver.phase)[2:end-1, 2:end-1]
            i, j = I.I

            <<calculate-left-hand-side>>
        end
    end
)
```

## 4 Numerical solver

```

        res = dL(solver, i,j ) \ b
        solver.phase[i, j] = res[1]
        solver.potential[i, j] = res[2]
    end
end
end

```

We denote the approximations for  $(\phi_{ij}^{n+1}, \mu_{ij}^{n+\frac{1}{2}})$  after smoothing, as  $(\bar{\phi}_{ij}^{n+1}, \bar{\mu}_{ij}^{n+\frac{1}{2}})$ . In Fig.4.1 we show 4 of the 7 initial data after one 200 iterations of smoothing. It is apparent that the sharp interface from the initial Data has diffused.

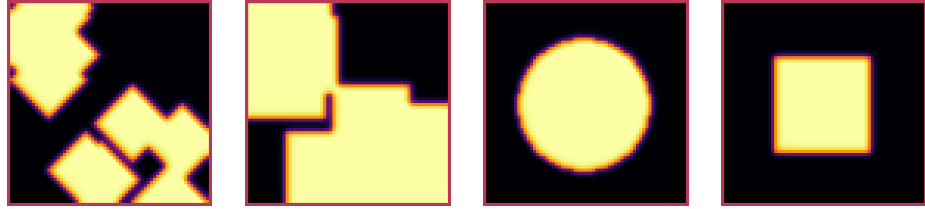


Figure 4.1: Inputs from 3.2 after SMOOTH.

## 4.2 TWO-GRID METHOD

The numerical method proposed in [1] consists of repeated sub-iterations of a multi-grid V-cycle. Specifically we use a two-grid implementation with a fixed number of sub-iterations. Defined as:

```

for j in 1:timesteps

    set_xi_and_psi!(solvers[1])

    for i = 1:subiterations

        v_cycle!(solvers, 1)
    end
end

```

The approximations for  $\phi_{ij}^{n+1}, \mu_{ij}^{n+\frac{1}{2}}$  after the m-th V-cycle sub-iteration are denoted with  $\phi_{ij}^{n+1,m+1}, \mu_{ij}^{n+\frac{1}{2},m+1}$  where m denotes the current sub-iteration Furthermore the V-cycle consists of the following setps:

### 4.2.1 PRE SMOOTHING

Pre smoothing consists of a fixed number of Gauss-Seidel iterations, in our case **40**, on the fine grid  $h$ , as described in Chapter 4.1. Afterwards we calculate the residual error  $(d_{ij,H}^{n+1,m}, r_{ij,H}^{n+1,m}) := L(\phi_{ij}^{n+1}, \mu_{ij}^{n+\frac{1}{2}}) - (\zeta_{ij}^n, \psi_{ij}^n)$  for the coarse grid  $H$  correction.

### 4.2.2 RESTRICTION

Restriction from the fine grid to the course grid  $h \rightarrow H$  for a variable eg.  $\phi_{ij}$  is done as follows:

$$\phi_{ij}^H = \frac{1}{\Sigma_{Gij}} \left( G_{2i,2j} \phi_{2i,2j}^h + G_{2i-1,2j} \phi_{2i-1,2j}^h + G_{2i,2j-1} \phi_{2i,2j-1}^h + G_{2i-1,2j-1} \phi_{2i-1,2j-1}^h \right) \quad (4.2)$$

### 4.2.3 COURSE GRID SOLUTION

On the course grid we use a Gauss-Seidel iteration to solve  $L(\hat{\phi}_{ij,H}^{n+1,m}, \hat{\mu}_{ij,H}^{n+\frac{1}{2},m})_H = L(\bar{\phi}_{ij,H}^{n+1,m}, \bar{\mu}_{ij,H}^{n+\frac{1}{2},m}) + (d_{ij,H}^{n+1,m}, r_{ij,H}^{n+1,m})$ . We solve for  $(\hat{\phi}_{ij,H}^{n+1,m}, \hat{\mu}_{ij,H}^{n+\frac{1}{2},m})$  using the same iteration as in Chapter 4.1 however we replace  $(\zeta_{ij}^n, \psi_{ij}^n)$  with  $L(\bar{\phi}_{ij,H}^{n+1,m}, \bar{\mu}_{ij,H}^{n+\frac{1}{2},m}) + (d_{ij,H}^{n+1,m}, r_{ij,H}^{n+1,m})$ . In the iteration, where  $(\bar{\phi}_{ij,H}^{n+1,m}, \bar{\mu}_{ij,H}^{n+\frac{1}{2},m})$  are the values after the smooth restricted to the coarser grid and  $(d_{ij,H}^{n+1,m}, r_{ij,H}^{n+1,m})$  is the residual from the smooth iteration on the fine grid restricted onto the coarse grid.

### 4.2.4 PROLONGATION

We prolong the solution from the course grid. Prolongation of a variable eg.  $\phi_{ij}$  from the course grid to the fine grid  $H \rightarrow h$  we do by using the nearest neighbour weighed by  $G$ .

$$\begin{pmatrix} \phi_{2i,2j}^h \\ \phi_{2i-1,2j}^h \\ \phi_{2i,2j-1}^h \\ \phi_{2i-1,2j-1}^h \end{pmatrix} = \begin{pmatrix} G_{2i,2j}^h \phi_{ij}^H \\ G_{2i-1,2j}^h \phi_{ij}^H \\ G_{2i,2j-1}^h \phi_{ij}^H \\ G_{2i-1,2j-1}^h \phi_{ij}^H \end{pmatrix} \quad (4.3)$$

## 4 Numerical solver

### 4.2.5 POST SMOOTHING

After prolongation of the coarse grid solution we perform a post smoothing step using **80** Gauss-Seidel steps. Post smoothing is otherwise identical to pre smoothing

### 4.2.6 ADDITIONAL CONSIDERATIONS

We Do Gauss-Seidel smoothing with fixed iterations. As well as a fixed number of sub-iterations.

The V-cycle of a two-grid method using pre- and post-smoothing is then stated by:

```
function alt_v_cycle!(grid::Array{T}, level) where T <: solver
    finegrid_solver = grid[level]
    #pre SMOOTHing
    SMOOTH!(solver, 40, false)

    d = zeros(size(finegrid_solver.phase))
    r = zeros(size(finegrid_solver.phase))

    # calculate error between L and expected values
    for I in CartesianIndices(finegrid_solver.phase)[2:end-1, 2:end-1]
        d[I], r[I] = [finegrid_solver.xi[I], finegrid_solver.psi[I]]
        .- L(finegrid_solver, I.I..., finegrid_solver.phase[I],
              ↳ finegrid_solver.potential[I])
    end

    restrict_solver!(grid[level], grid[level+1])
    coursegrid_solver = grid[level+1]
    solution = deepcopy(coursegrid_solver)

    d_large = restrict(d, G)
    r_large = restrict(r, G)

    u_large = zeros(size(d_large))
    v_large = zeros(size(d_large))

    for I in CartesianIndices(coursegrid_solver.phase)[2:end-1, 2:end-1]
        coursegrid_solver.xi[I] , coursegrid_solver.psi[I] = L(coursegrid_solver
          ↳ , I.I..., coursegrid_solver.phase[I] , coursegrid_solver.potential[I]
          ↳ ) .+ [d_large[I],r_large[I]]
    end
```

```

SMOOTH!(coursegrid_solver, 40 , false)

u_large = coursegrid_solver.phase .- solution.phase
v_large = coursegrid_solver.potential ..- solution.potential

finegrid_solver = grid[level]
finegrid_solver.phase .+= prolong(u_large , G)
finegrid_solver.potential .+= prolong(v_large, G)

SMOOTH!(finegrid_solver, 80, false)
end

```

```

function v_cycle!(grid::Array{T}, level) where T <: solver
    solver = grid[level]
    #pre SMOOTHing:
    SMOOTH!(solver, 400, false)

    d = zeros(size(solver.phase))
    r = zeros(size(solver.phase))

    # calculate error between L and expected values
    for I in CartesianIndices(solver.phase)[2:end-1, 2:end-1]
        d[I], r[I] = [solver.xi[I], solver.psi[I]] .- L(solver, I.I..., 
            ↪ solver.phase[I], solver.potential[I])
    end

    <<restrict-to-coarse-grid>>

    #Newton Iteration for solving smallgrid
    for i = 1:300
        for I in CartesianIndices(solver.phase)[2:end-1, 2:end-1]

            diffrence = L(solution, I.I..., solution.phase[I],
                ↪ solution.potential[I])
            .- [d_large[I], r_large[I]]
            .- L(solver, I.I..., solver.phase[I], solver.potential[I])

            local ret = dL(solution, I.I...) \ diffrence

            u_large[I] = ret[1]
            v_large[I] = ret[2]
        end
    end

```

## 4 Numerical solver

```
    solution.phase .-= u_large
    solution.potential .-= v_large
end

<<prolong-to-fine-grid>>

SMOOTH!(solver, 800, false)
end
```

After a few iterations, V-cycle exhibits the following behavior:

```
<<init>>
using JLD2
using DataFrames
results = jldopen("experiments/iteration.jld2")["result"]
anim = @animate for res in eachrow(results)
    heatmap(res.solver.phase , title="phase field" , legend=:none ,
            aspectratio=:equal , showaxis=false , grid=false , size=(400 ,400))
end
gif(anim , "images/iteration.gif" , fps = 10)

images/iteration.gif
```

# 5 NUMERICAL EXPERIMENTS

In the previous Chapter we discretized the CH equation based on the two-grid method described by the authors in [1] and we obtained a numerical scheme for  $\phi, \mu$ . In this chapter we analyze the change in mass, change in total energy  $E^{bulk}$ , the stability in time , space and during sub-iterations. Since we do not have exact solutions for the initial values tested, therefore we evaluate our solvers with a Cauchy criteria.

## 5.1 ENERGY EVALUATIONS

The discrete energy measure we use:

$$\begin{aligned} E_d^{\text{bulk}}(\phi_{ij}) &= \sum_{i,j \in \Omega} \frac{\varepsilon^2}{2} |G \nabla_d \phi_{ij}|^2 + W(\phi_{ij}) \\ &= \sum_{i,j \in \Omega} \frac{\varepsilon^2}{2} G_{i+\frac{1}{2}j} (D_x \phi_{i+\frac{1}{2}j})^2 + G_{ij+\frac{1}{2}} (D_y \phi_{ij+\frac{1}{2}})^2 + W(\phi_{ij}). \end{aligned} \quad (5.1)$$

Since the continuous total energy (2.2) decreases over time, we expect it's discrete counterpart to exhibit the same behaviour. Them numerical implementation for the bulk energy can be found in the Appendix 12.6. In Fig.5.1 we observe the discrete total energy going down with increasing number of time-steps, as we expect from a CH based solver. Visually we observe the energy decrease as reduced surface curvature.

## 5 Numerical experiments

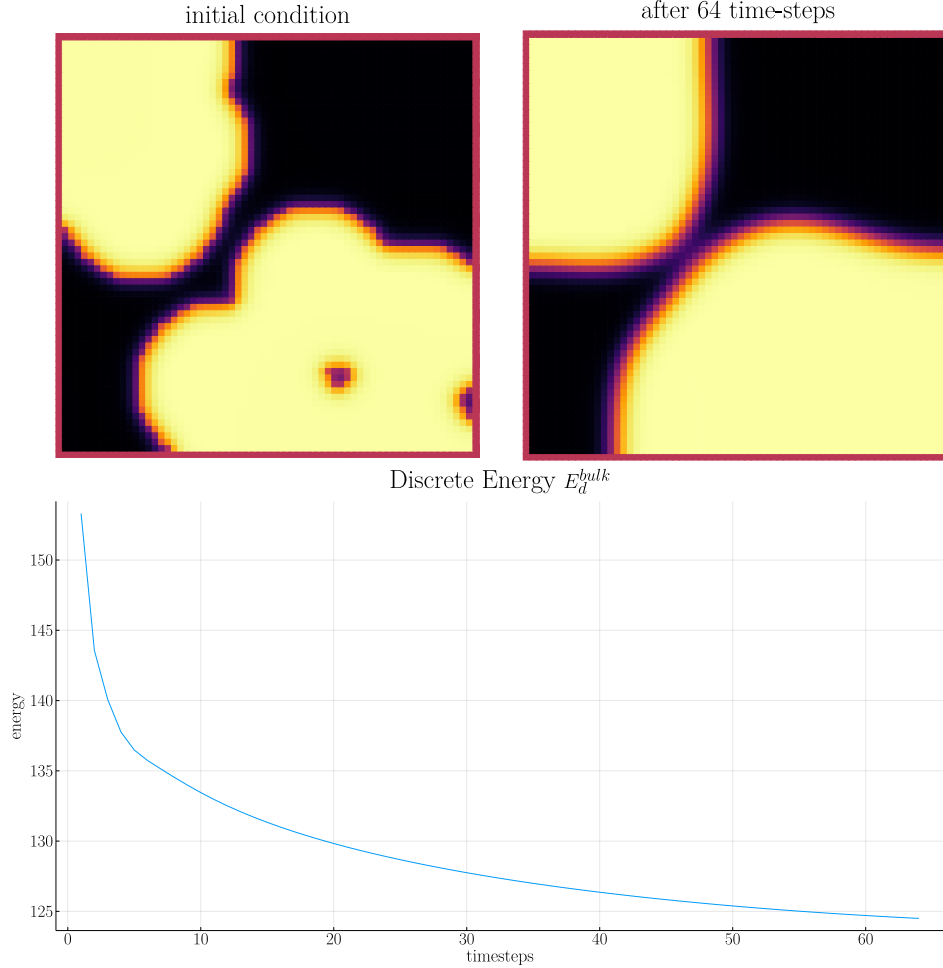


Figure 5.1: Behaviour of energy  $E_{bulk}$  over time for one initial condition  $\phi_0$ .

## 5.2 NUMERICAL MASS CONSERVATION

The analytical CH equation in (2.1) is mass conservative as shown in (2.7). Instead of a physical mass we use the average of  $\phi$  over the domain  $\Omega$ . This yields a balance between both phases. Since our implementation uses no-flow boundary conditions the balance between *phase 1* and *phase 2* stays the same. We therefore calculate a balance

$$b = \frac{\sum_{i,j \in \Omega} \phi_{ij}}{N^2}$$

such that  $b = 1$  means there only is phase 1,  $\phi \equiv 1$ , and  $b = -1$  means there is only phase 2,  $\phi \equiv -1$ . Ideally this value stays constant over time, for numerical mass conservation. In practice we observe slight fluctuations in Figure 5.2. Those however are close to machine precision and can therefore be ignored. The numerical implementation is in appendix 12.6.

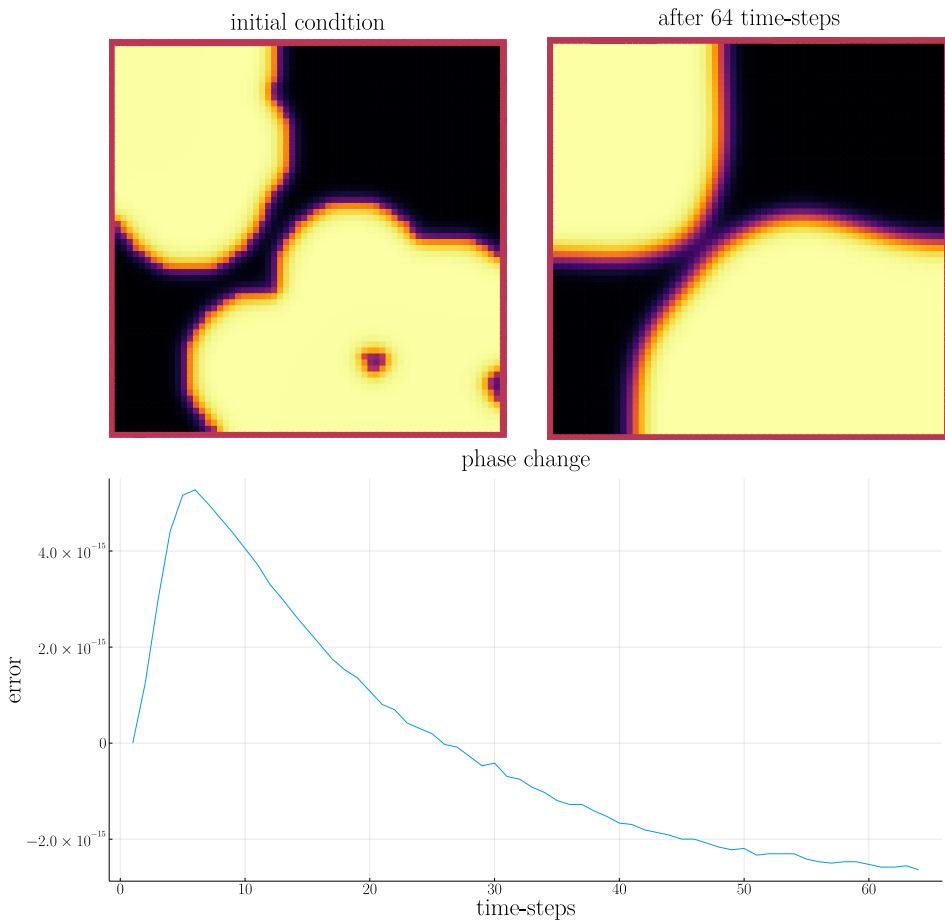


Figure 5.2: Behaviour of phase change over time for one initial condition  $\phi_0$ .

## 5 Numerical experiments

### 5.3 STABILITY OF A TWO-GRID SUB-ITERATION

We expect our solver to stay stable when increasing the number of two-grid sub-iterations. To validate this assumption we show convergence with the following Cauchy criteria.

$$\|\phi^{n+1,m-1} - \phi^{n+1,m}\|_{Fr} := \sqrt{\sum_{i,j \in \Omega_d} |\phi_{ij}^{n+1,m-1} - \phi_{ij}^{n+1,m}|^2} \quad (5.2)$$

We use similar criteria in the following sub chapters to show convergence for different hyperparameters. We expect sub-iterations to show Cauchy convergence, which is what we observe in Figure 5.3.

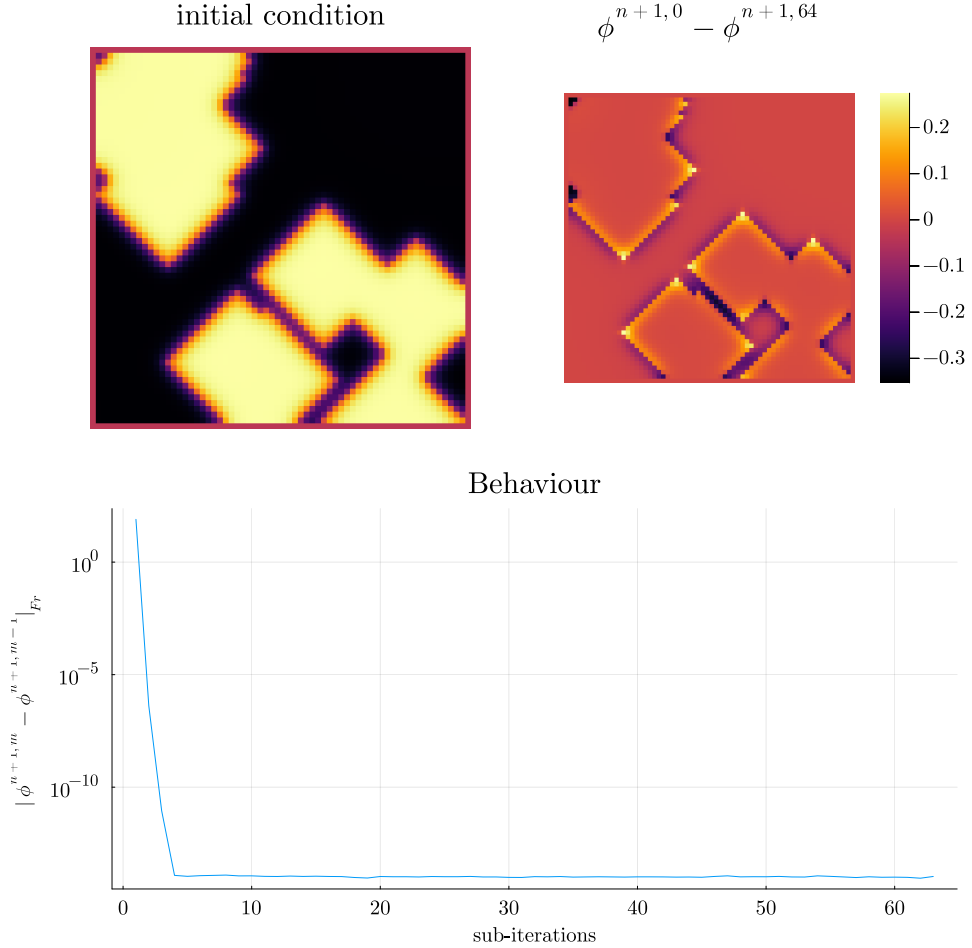


Figure 5.3: Stability of the original CH solver for increasing sub-iterations

During sub-iterations the convergence is exponential , and is reached at about 16 sub-iterations. The bend is only observed in the first time-step, and is likely due to the sharp interface in the initial values which is diffused during the first few sub-iterations. Looking at the difference before, and after one time step, it is apparent , that change is largest in areas with high curvature, which are mainly corners in the interface. Testing showed, that the number of sub-iterations required for convergence is dependant on the number of Gauss-Seidel iterations on each two-grud cycle. Though the general exponential behaviour stayed the same.

## 5.4 STABILITY IN TIME

We expect our numerical error to decrease when calculating with smaller time steps. To test this, we successively subdivide the original time interval  $[0, T]$  in finer parts. We fix  $\Delta t \cdot n = T$  for  $T = 10^{-2}$  and test different values of  $n$ . In Figure 5.4, as before, we employ a Cauchy criterai to compare the solution at  $T = 10^{-2}$ . We employ  $\|\phi^{n,64} - \phi^{n-1,64}\|_{Fr}$  as meassure.

## 5 Numerical experiments

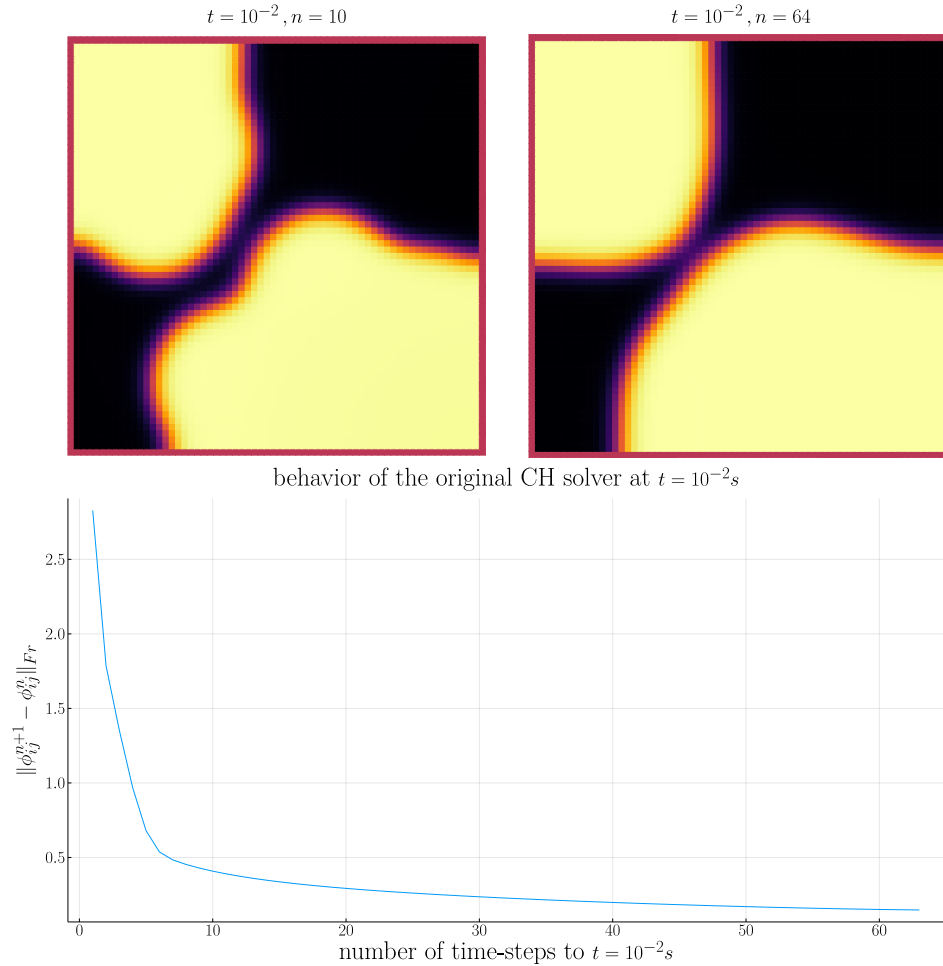


Figure 5.4: Behavior of the baseline solver while solving the time interval  $T = [0, 10^{-2}]$  with increasing number of time-steps.

## 5.5 STABILITY IN SPACE

We expect our methods to be stable under different grid-sizes  $h$  and grid-points  $N$ . Therefore we expect the difference after one time-step between eg. a  $512 \times 512$  grid and a  $1024 \times 1024$  grid to be smaller than the difference between a  $64 \times 64$  grid and a  $128 \times 128$  grid. In order to keep the problem the same , we fix  $Nh = 10^{-3} \cdot 1024$  and test for  $N \in \{1024, 512, 256, 128, 64, 32\}$  In Fig.5.5 we observe the differences to fluctuate between  $10^{-3}$  and  $10^{-4}$ . Indicating that the solver is somewhat stable.

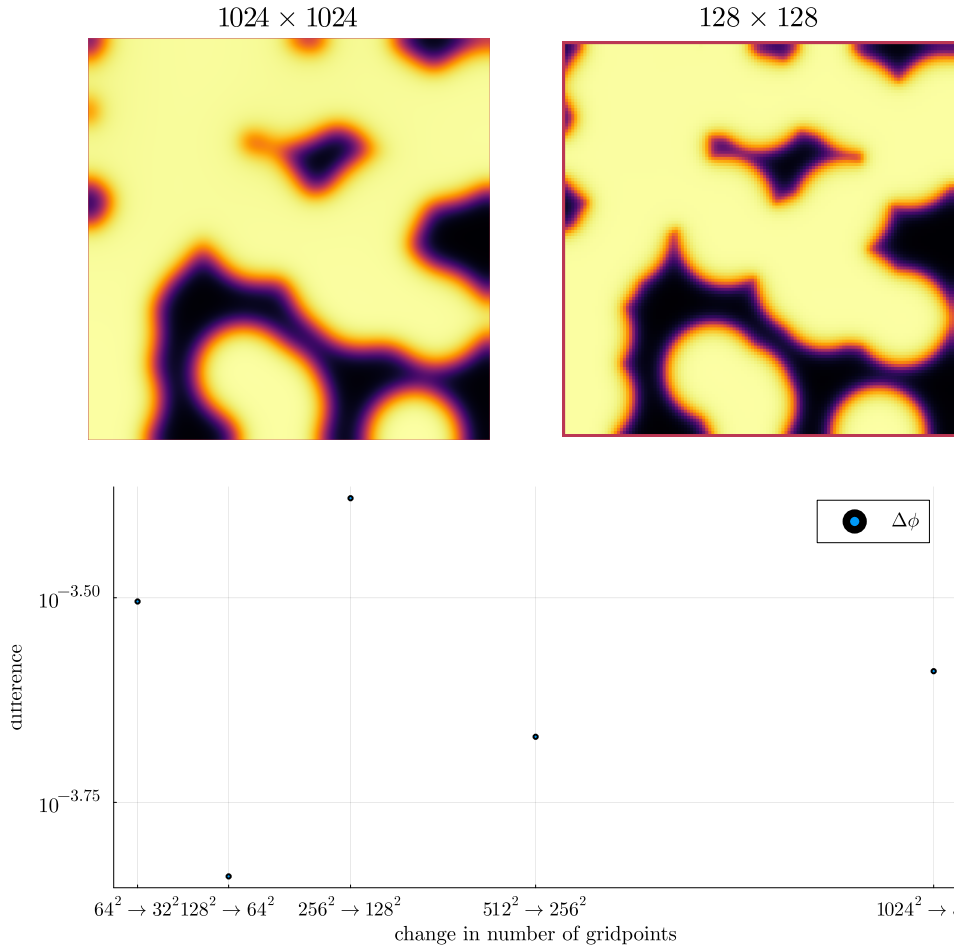


Figure 5.5: Behavior of the baseline solver while solving on successively finer grids



# 6 RELAXED CAHN-HILLIARD EQUATION

In effort to decrease the order of complexity, from fourth order derivative to second order, we propose an elliptical relaxation approach, where the relaxation variable  $c$  is the solution of the following elliptical PDE:

$$-\Delta c^\alpha + \alpha c^\alpha = \alpha \phi^\alpha, \quad (6.1)$$

where  $\alpha$  is a relaxation parameter. We expect to approach the original solution of the CH equation (2.1) as  $\alpha \rightarrow \infty$ . This results in the following relaxation for the classical CH equation (2.1):

$$\begin{aligned} \partial_t \phi^\alpha &= \Delta \mu, \\ \mu &= -\varepsilon^2 \alpha (c^\alpha - \phi^\alpha) + W'(\phi). \end{aligned} \quad (6.2)$$

It requires solving the elliptical PDE each time-step to calculate  $c$ .

## 6.1 RELAXED ENERGY FUNCTIONAL

We derive an corresponding energy for the relaxed CH eauation with the following inner product

$$\langle \phi_t^\alpha, \mu^\alpha \rangle = \langle \Delta \mu^\alpha, \mu^\alpha \rangle \quad (6.3)$$

it then follows for the left hand side

$$\begin{aligned} \langle \phi_t^\alpha, \mu^\alpha \rangle &= \langle \phi_t^\alpha, -\varepsilon^2 \alpha (c^\alpha - \phi^\alpha) + W'(\phi^\alpha) \rangle \\ &= \int_{\Omega} -\phi_t^\alpha \varepsilon^2 \alpha (c^\alpha - \phi^\alpha) d\mathbf{V} + \int_{\Omega} \phi_t^\alpha W'(\phi^\alpha) d\mathbf{V} \\ &= \frac{d}{dt} \int_{\Omega} -\frac{1}{2} \varepsilon^2 \alpha (c^\alpha - \phi^\alpha)^2 d\mathbf{V} + \frac{d}{dt} \int_{\Omega} W'(\phi^\alpha) d\mathbf{V} \\ &= \frac{d}{dt} \int_{\Omega} -\frac{1}{2} \varepsilon^2 \alpha (c^\alpha - \phi^\alpha)^2 d\mathbf{V} + \frac{d}{dt} \int_{\Omega} W(x) d\mathbf{V} =: \frac{d}{dt} E_{rel}(\phi^\alpha) \end{aligned} \quad (6.4)$$

## 6 Relaxed Cahn-Hilliard equation

and using the boundary condition  $\langle \nabla \mu, n \rangle = 0$  on the right hand side

$$\begin{aligned} \langle \Delta \mu^\alpha, \mu^\alpha \rangle &= \int_{\Omega} \mu^\alpha \Delta \mu^\alpha d\mathbf{x} \\ &= - \int_{\Omega} |\nabla \mu^\alpha| d\mathbf{V} + \int_{\partial\Omega} \mu^\alpha \langle \nabla \mu^\alpha, n \rangle d\mathbf{A} \\ &= -\|\nabla \mu^\alpha\| \leq 0 \end{aligned} \quad (6.5)$$

it therefore holds for a relaxed energy:

$$\frac{d}{dt} E_{rel}(\phi) = \frac{d}{dt} \int_{\Omega} -\frac{1}{2} \varepsilon^2 \alpha (c - \phi)^2 + W(x) d\mathbf{V} \leq 0 \quad (6.6)$$

which gives a bound for  $\Delta c = \alpha(c - \phi)$  similar to the estimate for  $\nabla \phi$  given in the original CH equation.

### 6.2 RELAXED MASS CONSERVATION

Identically to what was show for the original CH equation in (2.7) it holds:

$$\int_{\Omega} \partial_t \phi^\alpha d\mathbf{x} = \int_{\Omega} \Delta \mu^\alpha d\mathbf{x} = \int_{\partial\Omega} \nabla \mu^\alpha \cdot n d\mathbf{x} = 0 \quad (6.7)$$

The relaxed CH equation therefore is mass conservative.

### 6.3 RELAXED INITIAL VALUE PROBLEM

In this Thesis, regarding the relaxed CH equation, we concern our self with the following initial value problem, and it's numerical solution.

$$\begin{aligned} \partial_t \phi(x, t) &= \nabla \cdot \nabla \mu, \\ \mu^\alpha &= -\varepsilon^2 \alpha (c^\alpha - \phi^\alpha) + W'(\phi), \\ -\Delta c^\alpha + \alpha c^a &= \alpha \phi^\alpha, \\ -\nabla \mu^\alpha \cdot \mathbf{n} &= 0 && \text{on } \partial\Omega \times (0, T), \\ \nabla \phi^\alpha \cdot \mathbf{n} &= 0 && \text{on } \partial\Omega \times (0, T), \\ \nabla c^\alpha \cdot \mathbf{n} &= 0 && \text{on } \partial\Omega \times (0, T), \\ \phi^\alpha(x, 0) &= \phi^0(x), \\ c^\alpha(x, 0) &= \phi^0(x), \end{aligned} \quad (6.8)$$

# 7

## DISCRETIZATION OF THE RELAXED PROBLEM

As ansatz for the numerical solver for the CH equation we propose:

$$\begin{aligned} \frac{\phi_{ij}^{n+1,\alpha} - \phi_{ij}^{n,\alpha}}{\Delta t} &= \nabla_d \cdot (G_{ij} \nabla_d \mu_{ij}^{n+\frac{1}{2},\alpha}), \\ \mu_{ij}^{n+\frac{1}{2},\alpha} &= 2\phi_{ij}^{n+1,\alpha} - \varepsilon^2 a(c_{ij}^{n+1,\alpha} - \phi_{ij}^{n+1,\alpha}) + W'(\phi_{ij}^{n,\alpha}) - 2\phi_{ij}^{n,\alpha}. \end{aligned} \quad (7.1)$$

This approach is inspired by (3.7) and adapted to the relaxed CH equation in (7.1). We then apply the multi-grid method proposed in 4.2 to the relaxed problem by replacing the differential operators with their discrete counterparts, as defined in (3.4), and expand them. To solve the additional elliptical system, we propose a simple implicit finite difference scheme similar to what we use for the baseline solver.

$$-\nabla_d \cdot (G_{ij} \nabla_d c_{ij}^{n+1,\alpha}) + \alpha c_{ij}^{n+1,\alpha} = \alpha \phi_{ij}^{n+1,\alpha}$$

### 7.1 ELLIPTICAL PDE

We then use the finite differences defined in (3.4) to derive the corresponding linear system.

$$\begin{aligned} & -\frac{1}{h^2} (G_{i+\frac{1}{2}j}(c_{i+1j}^{n+1,\alpha} - c_{ij}^{n+1,\alpha}) \\ & + G_{ij+\frac{1}{2}}(c_{ij+1}^{n+1,\alpha} - c_{ij}^{n+1,\alpha}) \\ & + G_{i-\frac{1}{2}j}(c_{i-1j}^{n+1,\alpha} - c_{ij}^{n+1,\alpha})) \\ & + G_{ij-\frac{1}{2}}(c_{ij-1}^{n+1,\alpha} - c_{ij}^{n+1,\alpha}) + \alpha c_{ij}^{n+1,\alpha} = \alpha \phi_{ij}^{n+1,\alpha} \end{aligned}$$

## 7 Discretization of the relaxed problem

We abbreviate  $\Sigma_G c_{ij}^{n+1,\alpha} = G_{i+\frac{1}{2}j} c_{i+1j}^{n+1,\alpha} + G_{i-\frac{1}{2}j} c_{i-1j}^{n+1,\alpha} + G_{ij+\frac{1}{2}} c_{ij+1}^{n+1,\alpha} + G_{ij-\frac{1}{2}} c_{ij-1}^{n+1,\alpha}$  and  $\Sigma_{Gij} = G_{i+\frac{1}{2}j} + G_{i-\frac{1}{2}j} + G_{ij+\frac{1}{2}} + G_{ij-\frac{1}{2}}$ . Then the discrete elliptical PDE can be stated as:

$$-\frac{\Sigma_G c_{ij}^{n+1,\alpha}}{h^2} + \frac{\Sigma_G}{h^2} c_{ij}^{n+1,\alpha} + \alpha c_{ij}^{n+1,\alpha} = \alpha \phi_{ij}^{n+1,\alpha}. \quad (7.2)$$

this constitutes a linear system with  $N \times N$  equations

## 7.2 GAUSS SEIDEL SOLVER FOR THE ELLIPTICAL SYSTEM

To solve the elliptical system we introduce a Gauss-Seidel solver similar to the Gauss-Seidel Solver used for the smoothing step in the multi-grid method. We define this iteration in terms of  $s$ , For the Gauss-Seidel Iterative solver, we define the abbreviations

$$\Sigma_G c_{ij}^{n+1,\alpha,s+\frac{1}{2}} = G_{i+\frac{1}{2}j} c_{i+1j}^{n+1,\alpha,s} + G_{i-\frac{1}{2}j} c_{i-1j}^{n+1,\alpha,s+1} + G_{ij+\frac{1}{2}} c_{ij+1}^{n+1,\alpha,s} + G_{ij-\frac{1}{2}} c_{ij-1}^{n+1,\alpha,s+1}$$

We then define the gaus seidel iteration by the following, and solve algebraicly for  $c_{ij}^{n+1,\alpha,s+1}$

$$\begin{aligned} \left( \frac{\Sigma_{Gij}}{h^2} + \alpha \right) c_{ij}^{n+1,\alpha,s+1} &= \alpha \phi_{ij}^{n+1,\alpha} + \frac{\Sigma_G c_{ij}^{n+1,\alpha,s+\frac{1}{2}}}{h^2} \\ c_{ij}^{n+1,\alpha,s+1} &= \frac{\alpha \phi_{ij}^{n+1,\alpha} + \frac{\Sigma_G c_{ij}^{n+1,\alpha,s+\frac{1}{2}}}{h^2}}{\frac{\Sigma_G}{h^2} + \alpha} \\ c_{ij}^{n+1,\alpha,s+1} &= \frac{\alpha h^2 \phi_{ij}^{n+1,\alpha}}{\Sigma_{Gij} + \alpha h^2} + \frac{\Sigma_G c_{ij}^{n+1,\alpha,s+\frac{1}{2}}}{\Sigma_{Gij} + \alpha h^2} \end{aligned}$$

We run the elliptical solver for a fixed number of iterations. Furthermore we denote the solution of the iterative solver with  $c_{ij}^{n+1,\alpha}$ . We implement the corresponding iteration as follows:

```
function elyps_solver!(solver::T, n) where T <: Union{relaxed_multi_solver,
→ adapted_relaxed_multi_solver}
    for k in 1:n
        for i = 2:(solver.len+1)
            for j = 2:(solver.width+1)
```

```

bordernumber = neighbours_in_domain(i, j, G, solver.len,
                                     ↵ solver.width)
solver.c[i, j] =
(
    solver.alpha * solver.phase[i, j] +
    discrete_G_weighted_neighbour_sum(i, j, solver.c, G,
                                         ↵ solver.len, solver.width) / solver.h^2
) / (bordernumber / solver.h^2 + solver.alpha)

end
end
end
end

```

## 7.3 RELAXED SYSTEM

We use the same discretization approach, as for the baseline system. We reformulate the discretization in (7.1) in terms of the relaxed function  $L$  as follows:

$$L_r \begin{pmatrix} \phi_{ij}^{n+1,\alpha} \\ \mu_{ij}^{n+\frac{1}{2},\alpha} \end{pmatrix} = \begin{pmatrix} \frac{\phi_{ij}^{n+1,m,\alpha}}{\Delta t} - \nabla_d \cdot (G_{ji} \nabla_d \mu_{ji}^{n+\frac{1}{2},m,\alpha}) \\ \varepsilon^2 \alpha (c_{ij}^\alpha - \phi_{ij}^{n+1,m,\alpha}) - 2\phi_{ij}^{n+1,m,\alpha} - \mu_{ji}^{n+\frac{1}{2},m,\alpha} \end{pmatrix}$$

and its Jacobian:

$$DL_r \begin{pmatrix} \phi_{ij}^{n+1,\alpha,m} \\ \mu_{ij}^{n+\frac{1}{2},m,\alpha} \end{pmatrix} = \begin{pmatrix} \frac{1}{\Delta t} & \frac{1}{h^2} \Sigma_G \\ -\varepsilon^2 \alpha - 2 & 1 \end{pmatrix}$$

Much like the original solver, where in (3.10) we wrote the initial approach as as LES, we write the LES for the relaxed system as

$$L_r \begin{pmatrix} \phi_{ij}^{n+1,\alpha} \\ \mu_{ij}^{n+\frac{1}{2},\alpha} \end{pmatrix} = \begin{pmatrix} \zeta_{ij}^n \\ \psi_{ij}^n \end{pmatrix}, \quad (7.3)$$

where  $(\zeta_{ij}^n, \psi_{ij}^n)$  are the same in the original and relaxed solvers. Since the relaxed CH equation is no longer second order in both directions the resulting LES is simpler.

## 7 Discretization of the relaxed problem

To take advantage of this, we resolve the system algebraically for each grid-point  $(i,j)$ .

$$-\frac{\Sigma_{Gij}}{h^2} \mu_{ji}^{n+\frac{1}{2},m,\alpha} = \frac{\phi_{ij}^{n+1,m,\alpha}}{\Delta t} - \zeta_{ij}^{n,\alpha} - \frac{\Sigma_G \mu_{ij}}{h^2}, \quad (7.4)$$

$$\varepsilon^2 \alpha \phi_{ij}^{n+1,m,\alpha} + 2\phi_{ij}^{n+1,m,\alpha} = \varepsilon^2 \alpha c_{ij}^{n,\alpha} - \mu_{ji}^{n+\frac{1}{2},m,\alpha} - \psi_{ij}^{n,\alpha}, \quad (7.5)$$

where

- $\Sigma_G \mu_{ij} = G_{i+\frac{1}{2}j} \mu_{i+1j}^{n+\frac{1}{2},m} + G_{i-\frac{1}{2}j} \mu_{i-1j}^{n+\frac{1}{2},m} + G_{ij+\frac{1}{2}} \mu_{ij+1}^{n+\frac{1}{2},m} + G_{ij-\frac{1}{2}} \mu_{ij-1}^{n+\frac{1}{2},m}$ ,

The second dimension of (7.4) is solvable algebraically for  $\mu_{ij}^{n+\frac{1}{2},m,\alpha}$  and substitute it in (7.5).

$$\varepsilon^2 \alpha (\phi_{ij}^{n+1,m,\alpha}) + 2\phi_{ij}^{n+1,m,\alpha} = \varepsilon^2 \alpha c_{ij}^{n,\alpha} - \frac{h^2}{\Sigma_G} \left( \frac{\phi_{ij}^{n+1,m,\alpha}}{\Delta t} - \zeta_{ij}^n - \frac{1}{h^2} \Sigma_G \mu_{ij} \right) - \psi_{ij}$$

We solve this system for  $\phi_{ij}^{n+1,m,\alpha}$ . This results in the following system

$$\begin{aligned} \phi_{ij}^{n+1,m,\alpha} &= \left( \varepsilon^2 \alpha c_{ij}^{n,\alpha} - \frac{h^2}{\Sigma_G} \left( -\zeta_{ij}^n - \frac{\Sigma_G \mu_{ij}}{h^2} \right) - \psi_{ij} \right) \left( \varepsilon^2 \alpha + 2 + \frac{h^2}{\Sigma_G \Delta t} \right)^{-1} \\ \mu_{ij}^{n+\frac{1}{2},m,\alpha} &= \frac{h^2}{\Sigma_G} \left( \frac{\phi_{ij}^{n+1,m,\alpha}}{\Delta t} - \zeta_{ij}^n - \frac{1}{h^2} \Sigma_G \mu_{ij} \right) \end{aligned} \quad (7.6)$$

this system does no longer require solving a 2D LES in the gaus seidel implementation of the following chapter.

## 7.4 RELAXED GAUSS-SEIDEL ITERATION

We derive a gaus seidel iteration from (7.6). As before we state the iteration as.

$$\begin{aligned} \phi_{ij}^{n+1,\alpha,s+1} &= \left( \varepsilon^2 \alpha c_{ij}^{n,\alpha} - \frac{h^2}{\Sigma_G} \left( -\zeta_{ij}^n - \frac{\Sigma_G \mu_{ij}^{n+\frac{1}{2},\alpha,s+\frac{1}{2}}}{h^2} \right) - \psi_{ij}^n \right) \left( \varepsilon^2 \alpha + 2 + \frac{h^2}{\Sigma_G \Delta t} \right)^{-1} \\ \mu_{ij}^{n+\frac{1}{2},\alpha,s+1} &= \frac{h^2}{\Sigma_G} \left( \frac{\phi_{ij}^{n+1,\alpha,s+1}}{\Delta t} - \zeta_{ij}^n - \frac{1}{h^2} \Sigma_G \mu_{ij}^{n+\frac{1}{2},\alpha,s+\frac{1}{2}} \right) \end{aligned} \quad (7.7)$$

where

- $\Sigma_G \mu_{ij}^{n+\frac{1}{2},\alpha,s+\frac{1}{2}} = G_{i+\frac{1}{2}j} \mu_{i+1j}^{n+\frac{1}{2},s} + G_{i-\frac{1}{2}j} \mu_{i-1j}^{n+\frac{1}{2},s+1} + G_{ij+\frac{1}{2}} \mu_{ij+1}^{n+\frac{1}{2},s} + G_{ij-\frac{1}{2}} \mu_{ij-1}^{n+\frac{1}{2},s+1}$ ,

Contrary to the Gauss Seidel iteration in the baseline solver, this iteration is a significantly cheaper to calculate, since it no longer requires solving a 2x2 LES for each grid-point.

```
function SMOOTH!(
    solver::T,
    iterations,
    adaptive
) where T <: Union{relaxed_multi_solver , adapted_relaxed_multi_solver}
    for k = 1:iterations
        # old_phase = copy(solver.phase)
        for I in CartesianIndices(solver.phase)[2:end-1, 2:end-1]
            i, j = I.I
            <<solve-for-phi>>
            <<update-potential>>
        end

        #if adaptive && LinearAlgebra.norm(old_phase - solver.phase) < 1e-10
        ##println("SMOOTH terminated at $(k) successfully")
        #break
        #end
    end
end
```

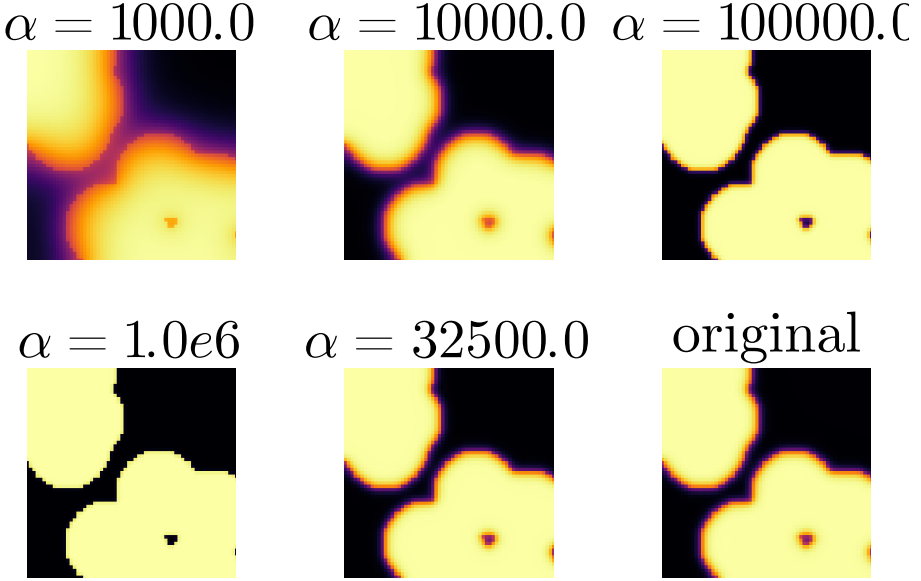


Figure 7.1: Effect of the relaxed SMOOTH operator, and additional solving of the elliptical problem, for different values of alpha

Furthermore, experimentation shows that alpha alone is insufficient to get a relaxed method consistent with the original solver, since  $\alpha$  had an effect similar to  $\varepsilon$ , where it changed the boundary thickness in the phase-field  $\phi$ . Therefore  $\varepsilon$  and  $\alpha$  cannot be chosen independently. Hence we use a simple Monte Carlo optimizer for  $\alpha, \varepsilon$  in order to give the relaxed solver the best chance we can. The implementation thereof is given in Appendix 12.5.

## 7.5 THE RELAXED MULTIGRID METHOD

As the difference between both methods is abstracted away in the operators, the relaxed V-cycle replaces the original operators with their relaxed counterparts. Due to julias multiple dispatch features this changes nothing in the implementation. Therefore we reuse the original V-cycle in the 4.2. In the executions for each time step, we add the elliptic solver in the subiteration. The iterative solver is then defined as:

```
for j in 1:timesteps
    set_xi_and_psi!(solvers[1])
```

```

for i = 1:subiterations

    elyps_solver!(solvers[1] , 1000)
    v_cycle!(solvers, 1)
end
end

```

[images/relaxed-anim.gif](#) The approach for the relaxed solver was in our tests significantly faster than the baseline implementation. The runtime in practice is highly dependant on the amount of v-cycle iteration for the baseline and relaxed solver respectively, as well as the number of Gauss-Seidel Iteration for the elliptical problem. When using similar sub iterations and sufficiently small the relaxed solver was several time faster. When we let both solvers iterate until convergence, the relaxed solver still was slightly faster. However, as we will show in our experiments the relaxed solver has problems with convergence, and never converges to the solution of the baseline. Because of this, and due to potential improvements in our implementation. The previous statements are to be taken as qualitative guide, and not as quantitative statement, which requires further research.



# 8 DISCRETE MASS CONSERVATION

Since both the CH equation (2.1) and the baseline solver from Fig.5.2 are mass conservative, the relaxed solver should be as well. Mass conservation for the CH equation is given as

$$\int_{\Omega} \partial_t \phi = 0 \quad (8.1)$$

We show a discrete analogue for both the baseline and the relaxed approach

$$\sum_{i,j \in \Omega_d} \frac{1}{\Delta t} (\phi_{ij}^{n+1} - \phi_{ij}^n) = 0. \quad (8.2)$$

We show this for a square domain  $\Omega_d$  using the first line of (3.7) and (7.1) respectively.

$$\sum_{i=2}^{N+1} \sum_{j=2}^{N+1} \frac{1}{\Delta t} (\phi_{ij}^{n+1} - \phi_{ij}^n) = \sum_{i=2}^{N+1} \sum_{j=2}^{N+1} \nabla_d \cdot (G_{ij} \nabla_d \mu_{ij}^{n+\frac{1}{2}}) \quad (8.3)$$

We split the right double sum into three parts. We consider them separately. The first part consists of the inner sum, where  $G_{i+\frac{1}{2}j} = G_{i+\frac{1}{2}j} = G_{ij+\frac{1}{2}} = G_{ij-\frac{1}{2}} = 0$ . The inner sum can therefore be written as such:

$$= \sum_{i=3}^N \sum_{j=3}^N \frac{1}{h^2} \left( \mu_{i+1j}^{n+\frac{1}{2}} + \mu_{i-1j}^{n+\frac{1}{2}} + \mu_{ij+1}^{n+\frac{1}{2}} + \mu_{ij-1}^{n+\frac{1}{2}} - 4\mu_{ij}^{n+\frac{1}{2}} \right) \quad (8.4)$$

## 8 Discrete mass conservation

The second part consists of the sums over the edges excluding the corners.

$$\begin{aligned}
& + \sum_{i=3}^N \frac{\Sigma_G \mu_{i2}^{n+\frac{1}{2}} - \Sigma_{Gi2} \cdot \mu_{i2}^{n+\frac{1}{2}}}{h^2} \\
& + \sum_{i=3}^N \frac{\Sigma_G \mu_{iN+1}^{n+\frac{1}{2}} - \Sigma_{GiN+1} \cdot \mu_{iN+1}^{n+\frac{1}{2}}}{h^2} \\
& + \sum_{j=3}^N \frac{\Sigma_G \mu_{i2}^{n+\frac{1}{2}} - \Sigma_{Gi2} \cdot \mu_{i2}^{n+\frac{1}{2}}}{h^2} \\
& + \sum_{j=3}^N \frac{\Sigma_G \mu_{N+1j}^{n+\frac{1}{2}} - \Sigma_{GN+1j} \cdot \mu_{N+1j}^{n+\frac{1}{2}}}{h^2}
\end{aligned} \tag{8.5}$$

And the third part consists of the corners.

$$\begin{aligned}
& + \frac{\Sigma_G \mu_{N+1N+1}^{n+\frac{1}{2}} - \Sigma_{GN+1,N+1} \cdot \mu_{N+1,N+1}^{n+\frac{1}{2}}}{h^2} \\
& + \frac{\Sigma_G \mu_{N+1,2}^{n+\frac{1}{2}} - \Sigma_{GN+1,2} \cdot \mu_{N+1,2}^{n+\frac{1}{2}}}{h^2} \\
& + \frac{\Sigma_G \mu_{2,N+1}^{n+\frac{1}{2}} - \Sigma_{G2,N+1} \cdot \mu_{2,N+1}^{n+\frac{1}{2}}}{h^2} \\
& + \frac{\Sigma_G \mu_{2,2}^{n+\frac{1}{2}} - \Sigma_{G2,2} \cdot \mu_{2,2}^{n+\frac{1}{2}}}{h^2}
\end{aligned} \tag{8.6}$$

The first double sum is a telescopic sum, and contracts to the following:

$$\begin{aligned}
\sum_{i=3}^N \sum_{j=3}^N \frac{1}{h^2} \left( \mu_{i+1j}^{n+\frac{1}{2}} + \mu_{i-1j}^{n+\frac{1}{2}} + \mu_{ij+1}^{n+\frac{1}{2}} + \mu_{ij-1}^{n+\frac{1}{2}} - 4\mu_{ij}^{n+\frac{1}{2}} \right) & = \sum_{i=3}^N \mu_{i2}^{n+\frac{1}{2}} - \mu_{i3}^{n+\frac{1}{2}} \\
& + \sum_{i=3}^N \mu_{iN+1}^{n+\frac{1}{2}} - \mu_{iN}^{n+\frac{1}{2}} \\
& + \sum_{j=3}^N \mu_{2j}^{n+\frac{1}{2}} - \mu_{3j}^{n+\frac{1}{2}} \\
& + \sum_{j=3}^N \mu_{N+1j}^{n+\frac{1}{2}} - \mu_{Nj}^{n+\frac{1}{2}}
\end{aligned} \tag{8.7}$$

Additionally, we simplify each of the sums in the second part, since the values of  $G$  are known on the boundary. On the right boundary ,for  $2 < i < N + 1$ ,  $G_{iN+\frac{3}{2}} = 0$  and  $G_{iN+\frac{1}{2}} = G_{i+\frac{1}{2}N+1} = 1$  it therefore follows:

$$\begin{aligned}
\sum_{i=3}^N \frac{\Sigma_G \mu_{iN+1}^{n+\frac{1}{2}} - \Sigma_{GiN+1} \cdot \mu_{iN+1}^{n+\frac{1}{2}}}{h^2} &= \frac{1}{h^2} \sum_{i=3}^N G_{i+\frac{1}{2}N+1} \mu_{i+1N+1}^{n+\frac{1}{2}} + G_{i-\frac{1}{2}N+1} \mu_{i-1N+1}^{n+\frac{1}{2}} \\
&\quad + G_{iN+\frac{3}{2}} \mu_{iN+2}^{n+\frac{1}{2}} + G_{iN-\frac{3}{2}} \mu_{iN}^{n+\frac{1}{2}} \\
&\quad - (G_{iN+\frac{3}{2}} + G_{iN+\frac{1}{2}} + G_{i+\frac{1}{2}N+1} + G_{i-\frac{1}{2}N+1}) \mu_{iN+1}^{n+\frac{1}{2}} \\
&= \frac{1}{h^2} \sum_{i=3}^N \mu_{i+1N+1}^{n+\frac{1}{2}} + \mu_{i-1N+1}^{n+\frac{1}{2}} + \mu_{iN}^{n+\frac{1}{2}} - 3\mu_{iN+1}^{n+\frac{1}{2}}
\end{aligned} \tag{8.8}$$

this sum, as it is telescopic simplify further to

$$\begin{aligned}
\sum_{i=3}^N \frac{\Sigma_G \mu_{iN+1}^{n+\frac{1}{2}} - \Sigma_{GiN+1} \cdot \mu_{iN+1}^{n+\frac{1}{2}}}{h^2} &= (\mu_{NN+1} + \mu_{3N+1}) - (\mu_{N+1N+1} + \mu_{2N+1}) \\
&\quad - \sum_{i=3}^N \mu_{i1N}^{n+\frac{1}{2}} - \mu_{iN+1}^{n+\frac{1}{2}}
\end{aligned} \tag{8.9}$$

similar the other three sums on the boundary simplify to

$$\begin{aligned}
\sum_{i=3}^N \frac{\Sigma_G \mu_{i2}^{n+\frac{1}{2}} - \Sigma_{Gi2} \cdot \mu_{i2}^{n+\frac{1}{2}}}{h^2} &= (\mu_{N,2} + \mu_{3,2}) - (\mu_{N+1,2} + \mu_{2,2}) - \sum_{i=3}^N \mu_{i1N}^{n+\frac{1}{2}} - \mu_{iN+1}^{n+\frac{1}{2}} \\
\sum_{j=3}^N \frac{\Sigma_G \mu_{2j}^{n+\frac{1}{2},\alpha} - \Sigma_{G2j} \cdot \mu_{2j}^{n+\frac{1}{2}}}{h^2} &= (\mu_{2,3} + \mu_{2,N}) - (\mu_{2,N+1} + \mu_{2,2}) - \sum_{j=3}^N \mu_{2j}^{n+\frac{1}{2}} - \mu_{3j}^{n+\frac{1}{2}} \\
\sum_{j=3}^N \frac{\Sigma_G \mu_{N+1j}^{n+\frac{1}{2}} - \Sigma_{GN+1j} \cdot \mu_{N+1j}^{n+\frac{1}{2}}}{h^2} &= (\mu_{N+1,N} + \mu_{N+1,3}) - (\mu_{N+1,N+1} + \mu_{N+1,2}) - \sum_{j=3}^N \mu_{N+1,j}^{n+\frac{1}{2}} - \mu_{N,j}^{n+\frac{1}{2}}
\end{aligned} \tag{8.10}$$

we observe that the resulting sums are equal and oposite to the result from the first sum. They therefore cancel each other and we are left with the corner therms. Those therms sum up to

$$\mu_{N+1,N} + \mu_{N+1,3} - 2\mu_{N+1,N+1} + \mu_{2,3} + \mu_{2,N} - 2\mu_{2,2} + \mu_{N,2} + \mu_{N+1,3} - 2\mu_{2,N+1} + \mu_{N,N+1} + \mu_{3,N+1} - 2\mu_{N+1,2} \tag{8.11}$$

## 8 Discrete mass conservation

The third sum, on the corners, can be simplified the same way as the other two

$$\begin{aligned}
 \frac{\Sigma_G \mu_{N+1,N+1}^{n+\frac{1}{2}} - \Sigma_{G(N+1,N+1)} \cdot \mu_{N+1,N+1}^{n+\frac{1}{2}}}{h^2} &= \frac{1}{h^2} (\mu_{NN+1}^{n+\frac{1}{2}} + \mu_{N+1N}^{n+\frac{1}{2}} - 2\mu_{N+1N}^{n+\frac{1}{2}}) \\
 \frac{\Sigma_G \mu_{2,2}^{n+\frac{1}{2}} - \Sigma_{G(2,2)} \cdot \mu_{2,2}^{n+\frac{1}{2}}}{h^2} &= \frac{1}{h^2} (\mu_{3,2}^{n+\frac{1}{2}} + \mu_{2,3}^{n+\frac{1}{2}} - 2\mu_{2,2}^{n+\frac{1}{2}}) \\
 \frac{\Sigma_G \mu_{2N+1}^{n+\frac{1}{2}} - \Sigma_{G(2,N+1)} \cdot \mu_{2,N+1}^{n+\frac{1}{2}}}{h^2} &= \frac{1}{h^2} (\mu_{3N+1}^{n+\frac{1}{2}} + \mu_{2N}^{n+\frac{1}{2}} - 2\mu_{2N+1}^{n+\frac{1}{2}}) \\
 \frac{\Sigma_G \mu_{N+1,2}^{n+\frac{1}{2}} - \Sigma_{G(N+1,2)} \cdot \mu_{N+1,2}^{n+\frac{1}{2}}}{h^2} &= \frac{1}{h^2} (\mu_{N+1,3}^{n+\frac{1}{2}} + \mu_{N,2}^{n+\frac{1}{2}} - 2\mu_{N+1,2}^{n+\frac{1}{2}})
 \end{aligned} \tag{8.12}$$

Those terms cancel out with what remains in the second sum. We therefore conclude

$$\sum_{i=2}^{N+1} \sum_{j=2}^{N+1} \frac{1}{\Delta t} (\phi_{ij}^{n+1} - \phi_{ij}^n) = 0 \tag{8.13}$$

Which gives a discrete equivalent to the mass conservation shown in the analytical equations.

# 9 RELAXED EXPERIMENTS

We expect the relaxed solver to behave the same as the baseline method for all test cases that we have introduced in Chapter 5. Therefore we run the same experiments for our relaxed solver.

## 9.1 RELAXED ENERGY EVALUATIONS

we do evaluate our relaxed method using the discrete energy defined in (5.1). On the same initial data, and with the same values for  $\varepsilon, h, dt$  as in the Chapter 5.1. Since we expect the relaxed approach to solve the same initial value problem (2.8), we expect both solvers to behave the same. In Figure 9.1 we then observe the energy decay we expected. Our relaxed approach closely follows the baseline, although it consistently decays slightly faster. Both solvers decay in a similar manner and both solvers show a slight bend after a few iterations. However the bend in the relaxed solver is noticeably more pronounced. Additionally, in later iterations the relaxed solver shows faster energy decay than the original. We explain these differences with the observations taken in later experiments, where we observe mass-loss and slower convergence. We suspect the relaxed solver to therefore be more aggressive when minimizing energy.

## 9 Relaxed experiments

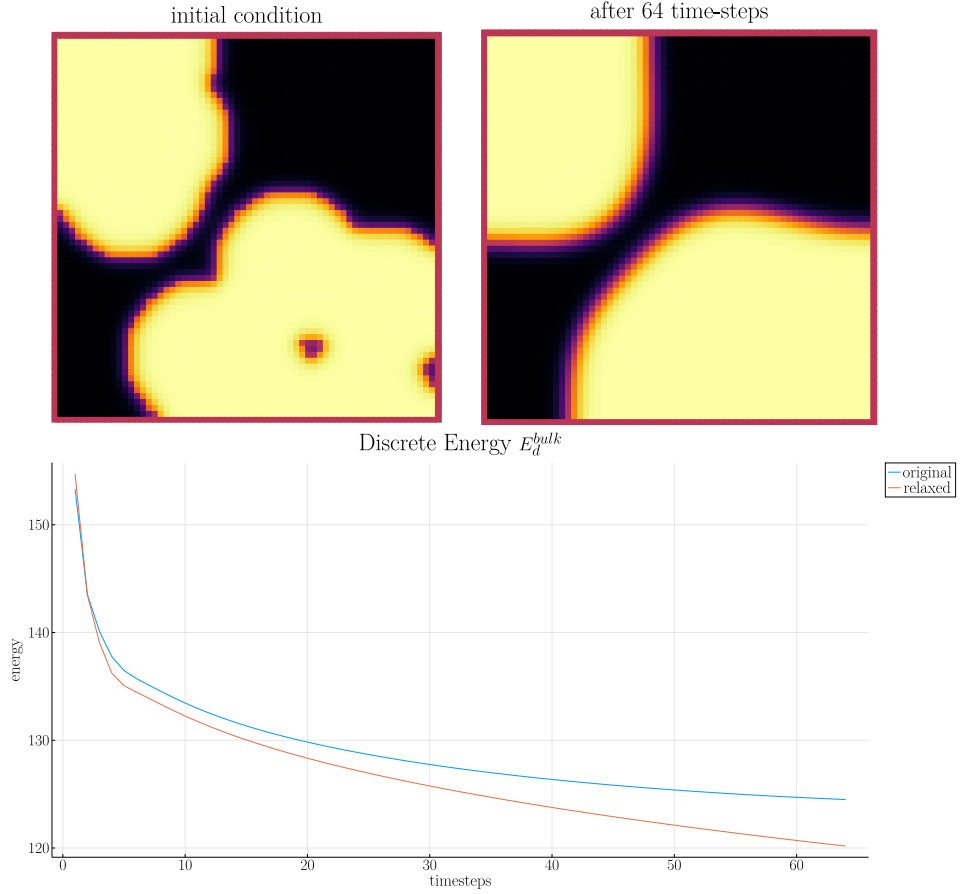
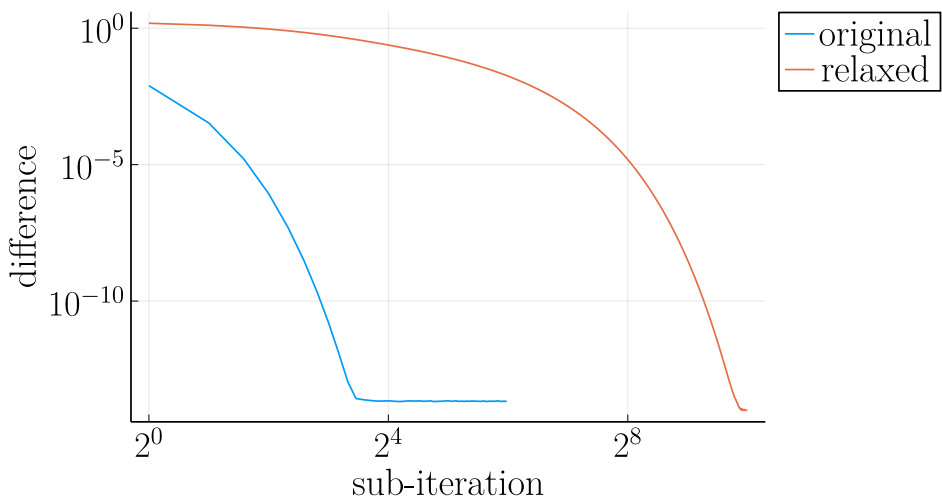


Figure 9.1: Energy decay of the relaxed solver compared to the original solver.

## 9.2 STABILITY OF A RELAXED MULTIGRID SUB-ITERATION

We use the same Cauchy criteria we used for the baseline solver. Furthermore, we compare the subiteration behaviour of the relaxed solver to the original we therefore plot  $\|\phi_{ij}^{n+1,m} - \phi_{ij}^{n+2,m-1}\|_{Fr}$  against  $\|\phi_{ij}^{n+1,m,\alpha} - \phi_{ij}^{n+1,m-1,\alpha}\|$  for  $m \in \{2, \dots, 64\}$ . The sub-iterations in Fig. 9.2 are stable. However, the relaxed solver shows significantly slower convergence compared to the baseline solver. Which is why without the log log scale employed, the behavior of both solvers would not be visible in the same plot. This behaviour suggests that the relaxed solver does not converge towards the solution of (7.6). Further experiments on mass conservation confirm this suspicion. During further experiments with different initial conditions and number of Gauss-Seidel steps, we were not able to change the slow convergence behaviour.



### 9.3 RELAXED NUMERICAL MASS BALANCE

As already mentioned the relaxed solver is not mass conservative. Our relaxed solver shows significant mass loss as seen in Fig.9.2. especially when compared to the original solver as seen in Fig.5.2. The relaxed solver is therefore not mass conservative. Both the original approach as well as the relaxed one exhibit a discrete equivalent of mass conservation, therefore their difference has to be explained by the numerical solver. Which is consistent with the observations made with sub-iteration convergence. We therefore conclude our relaxed solver does not properly converge. This, most likely, is due to our choice of alternating the solution of  $c$  and  $\phi$ . Especially since we intend to solve them both implicitly. Coupling the elliptical and relaxed CH equation might alleviate this, however the resulting system would be of similar complexity than (3.8), which is what we intend to prevent with the relaxation approach. Alternatively, solving  $c$  explicitly leads to an unstable solver with the initial conditions used by us. We didn't test different initial conditions due to a lack of computational resources and time.

## 9 Relaxed experiments

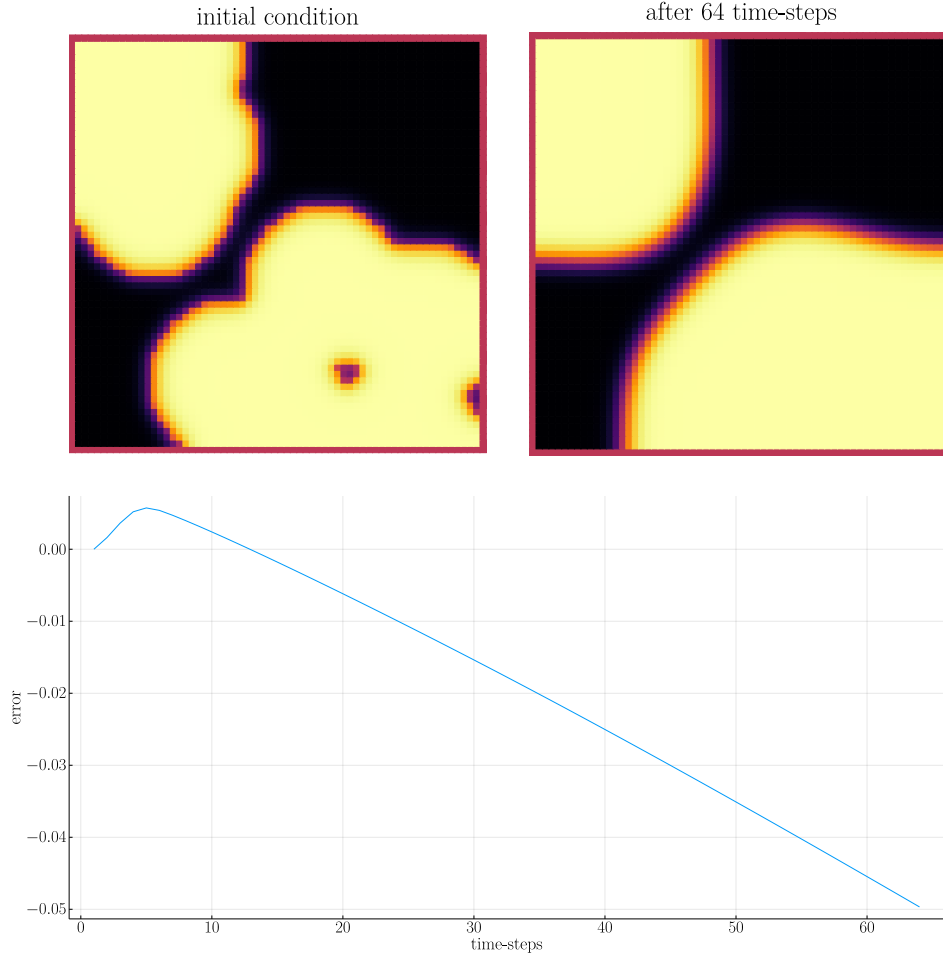


Figure 9.2: Mass loss in the relaxed solver

## 9.4 RELAXED STABILITY IN TIME

we test the behaviour under refinement in time by successive subdividing of the original time interval  $[0, T]$  into finer parts. We use the same measure as in Chapter 5.4 and directly compare. We observe similar behaviour to the original solver in Fig. 9.3. The relaxed solver is consistently lower than the original solver. This might suggest a more consistent method over time.

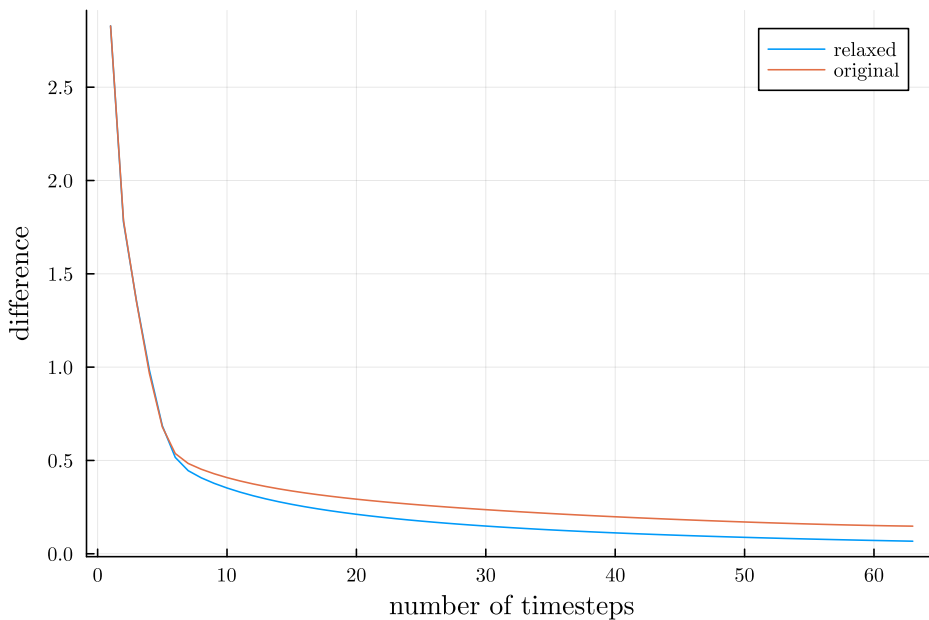


Figure 9.3: Behavior of the relaxed and baseline solvers while solving the time interval  $t \in [0, 10^{-2}]$  with increasing number of time-steps.

## 9.5 RELAXED STABILITY IN SPACE

For the relaxed solver we do the same evaluation for space, that we did for the baseline solver. We  $\Delta\phi$  going down exponentially with increasing grid sizes. This behaviour is as expected. However the jump from  $128^2 \rightarrow 64^2$  to  $256^2 \rightarrow 128^2$  leads us to believe, that the solver is not yet stable for courser grids.



# 10 COMPARISON

In the previous chapter we have shown the stability for both solver. In this chapter we show a direct comparison between both methods.

## 10.1 EFFECT OF ALPHA

To see the impact of  $\alpha$  on our solver, we evaluate both solvers after one time-step , and then calculate the difference between  $\phi_{ij}^{n+1}$  and  $\phi_{ij}^{n+1,\alpha}$ , for various values of  $\alpha$ . Since the solution of the relaxed solver should approach the original solver, we expect

$$\|\phi_{ij}^{n+1} - \phi_{ij}^{n+1,\alpha}\|_{Fr} \rightarrow 0. \quad (10.1)$$

In Fig.10.1 we observe the following behaviour where in all cases the difference between the relaxed solver and the original solver is apparent. Furthermore we observe a optimal value of  $\alpha$  at approximately  $7.5 * 10^5$ . We explain this with our observations done for the Smoothing operator, where for small and large values of  $\alpha$  the relaxed solver results in restricted behaviour, which we also expect. On the other hand, for large values of  $\alpha$  the elliptical equation approaches  $\phi$ , however it does not converge to  $\phi$  for small values of  $\alpha$ .

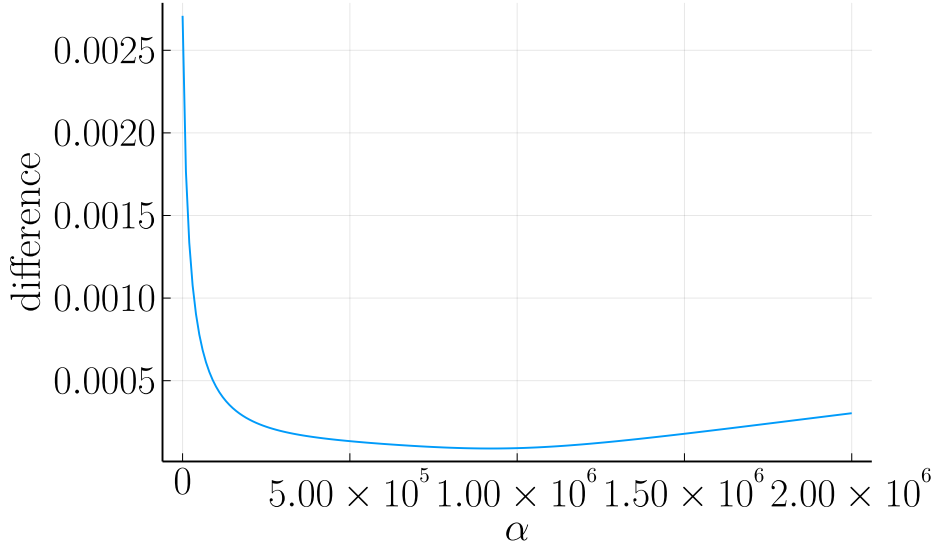


Figure 10.1: Difference between the original solver  $\phi_{ij}^1$  and the relaxed solver  $\phi_{ij}^{1,\alpha}$  for different values of  $\alpha$

## 10.2 DIRECT COMPARISON

We then show a comparison of both solvers we plot the phase-fields after 64 time-steps, and the difference  $\|\phi_{ij}^{n+1} - \phi_{ij}^{n+1,\alpha}\|_{Fr}$  over the time-steps  $n \in \{0, \dots, 63\}$ . We can observe slight differences between the original solver and the relaxed solver. To quantify those, we run the relaxed solver for a fixed value of  $\alpha = 7700$ , as it is in the intervall where  $\alpha$  is minimal in Fig.10.1. We then show the numerical difference between  $\phi_{ij}^n$  and  $\phi_{ij}^{n,\alpha}$  in Fig.10.2. The observed difference is mainly in areas with high curvature and inclusions of small segments of one phase in the other.

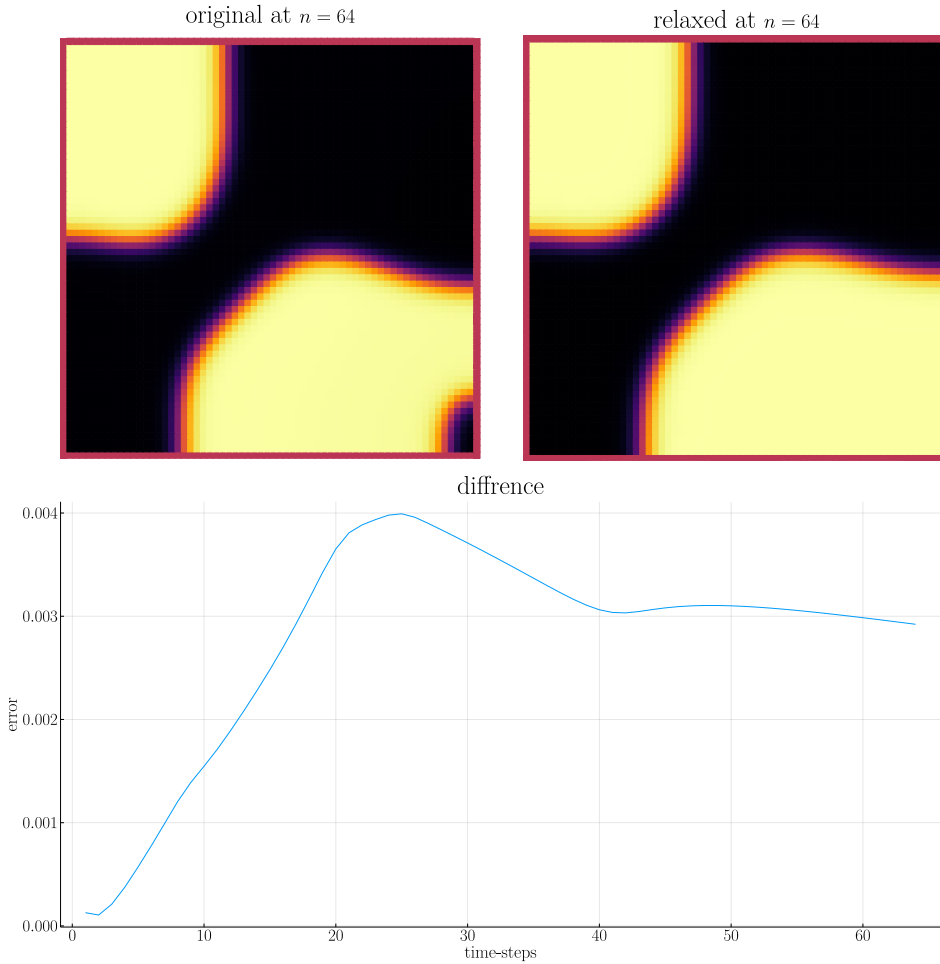


Figure 10.2: Comparison between the original and the relaxed CH solvers.

### 10.3 OPTIMIZER FOR ALPHA

In addition to the experiments in Fig.10.1 we have experimented with a Monte Carlo Optimizer to optimize  $\alpha$  in conjunction with  $\varepsilon$ , to best approximate the baseline solver after one time-step. This resulted in a optimal  $\varepsilon$  found that was very close to the actual  $\varepsilon$  used. (9e-3 compared to 8e-3). This gives us confidence that the relaxed method solves the same problem, as the baseline. Optimal values for  $\alpha$  varied , however stayed fairly large around  $10^5 \rightarrow 10^6$ .



# 11 CONCLUSION

In this thesis we have presented a simple introduction to the CH equation and have shown two numerical solvers for it. We have presented a baseline method implemented from the authors [1], and have shown how to derive it from their initial approach. We have done the derivations in a way, that enables a simple adaptation to a modified version of the discrete CH equation (3.7), as introduced in [1]. We have introduced measures to evaluate both solvers in space, time and mass conservation as well as their sub-iteration behaviour. We have shown the baseline to be mass conservative, in a numerical sense, and we have shown it to be stable in all tested measures. We have shown our relaxed solver to approach the baseline, during sub-iterations it converges significantly slower than the baseline solver. Furthermore it is not mass conservative. We intentionally didn't evaluate runtime since numerical experiments have shown both solvers to be dependant on the amount of sub-iterations, hyperparameters such as  $\varepsilon$  as well as the number of smoothing iterations. It would therefore be unfair to evaluate one solver on a set of parameters tweaked for the other. As example for this dilemma we recall runs where the relaxed solver was around 10x faster than the baseline with the same parameters. The baseline solver was able to run with 10x less smoothing iterations than the relaxed one. A fair comparison would hence require to find the optimal number of smoothing for each solver.

For the sake of completeness we include runtime benchmarks of both methods. Those should be taken with a pinch of salt because of the reasons above. Both examples are run with the same parameters and the results are in the Appendix.

## 11.1 OUTLOOK

This thesis leaves a lot of room for further research. We have already mentioned runtime evaluations, which require more optimizations, and additional experiments to test the number of smoothing iterations. Here it would be beneficial if both solvers are made adaptive, to ensure fair evaluations. Furthermore, we initially considered a

## *11 Conclusion*

machine learning approach to replace the elliptical system. We didn't follow this idea mostly due to time constraints, as we had already collected trainings data during our numerical experiments. Our choice of programming language would have been of benefit here, as it would enable more advanced techniques, such as integrating the numerical solver in the trainings loop since Julia offers automatic differentiation of arbitrary functions, and therefore enables back-propagation (gradient descent) through the entire solver. Interessting would also have been different discretizations of the relaxed CH equation, and different method for solving it, such as a finite volume or finite element method. Those bring the chalange of being harder to compare to our baseline.

# 12 APPENDIX

## 12.1 OPERATOR IMPLEMENTATION

### 12.1.1 RELAXED

```
function L(solver::relaxed_multi_solver,i,j , phi , mu)
    xi = solver.phase[i, j] / solver.dt -
        (discrete_G_weighted_neighbour_sum(i, j, solver.potential, G, solver.len,
        ↵ solver.width)

    -
    neighbours_in_domain(i, j, G, solver.len, solver.width) * mu
    ↵ )/solver.h^2
    psi = solver.epsilon^2 * solver.alpha*(solver.c[i,j] - phi) -
        ↵ solver.potential[i,j] - 2 * solver.phase[i,j]
    return [xi, psi]
end

function dL(solver::relaxed_multi_solver , i , j)
    return [ (1/solver.dt) (1/solver.h^2*neighbours_in_domain(i,j,G,solver.len ,
    ↵ solver.width));
        (-1*solver.epsilon^2 * solver.alpha - 2) 1]
end
```

## 12.2 RNG GENERATION

for random point generation we use the folowing Function and seed.

2×12 Matrix{Int64}:

48	40	20	1	63	49	8	60	26	58	26	11
17	13	56	52	15	9	30	14	40	9	40	25

the random testdata is then generated as follows

## 12.3 ALTERNATIVE EXPERIMENTS

### 12.3.1 ITERATION

```

using JLD2
using DataFrames
using Random
using ProgressMeter
include(pwd() * "/src/solvers.jl")
include(pwd() * "/src/adapted_solvers.jl")
include(pwd() * "/src/utils.jl")
include(pwd() * "/src/multisolver.jl")
include(pwd() * "/src/multi_relaxed.jl")
include(pwd() * "/src/testgrids.jl")
include(pwd() * "/src/elypssolver.jl")
using Plots
using LaTeXStrings
using LinearAlgebra
using Printf
using ProgressBars
default(fontfamily="computer modern" , titlefontsize=32 , guidefontsize=22 ,
→ tickfontsize = 22 , legendfontsize=22)
pgfplotsx()
layout2x2 = grid(2,2)
layout3x1 = @layout [ b c ; a]
size3x1 = (1600,1600)
SIZE = 64
M = testdata(SIZE, SIZE ÷ 5, SIZE /5 , 2)

incirc(M) = filter(x -> norm(x.I .- (size(M, 1) / 2, size(M, 2) / 2)) <
→ min(size(M)... ) / 3, CartesianIndices(M))
insquare(M) = filter(x -> norm(x.I .- (size(M, 1) / 2, size(M, 2) / 2), Inf) <
→ min(size(M)... ) / 4, CartesianIndices(M))
side(M) = filter(x -> x.I[2] < size(M, 2) ÷ 2, CartesianIndices(M))
halfcirc(M) = filter(x -> norm(x.I .- (1, size(M, 2) / 2), 2) < min(size(M)... ) /
→ 3, CartesianIndices(M))

function get_special_input(fn, size)
    M = fill(-1, size , size )
    M[fn(M)] .= 1
    return M
end
SIZE =64
t1= [testdata(SIZE, SIZE ÷ 5, SIZE /5 , j) for j in [1,2, Inf]]

```

```

t2 = [get_special_input(fn,SIZE) for fn in [halfcirc , incirc, side , insquare]]
initial_data = [t1 ; t2]
tests = [testgrid(multi_solver, M , 2) for M in initial_data]

n = 64
m = 16
function iter(g::Vector{T} , experiment , prg::Progress) where T<: solver
    out = []
    for j in 1:n
        set_xi_and_psi!(g[1])
        for i = 1:m
            alt_v_cycle!(g, 1)
            next!(prg)
        end
        push!(out, (solver=deepcopy(g[1]), iteration=j , experiment=experiment))
    end
    return out
end

prg=Progress(size(tests ,1)*n*m , showspeed=true , )
tasks = []
for i in eachindex(tests)
    t = Threads.@spawn iter(tests[i], i , prg)
    push!(tasks , (iteration = 1 , task = t))
end
result = DataFrame()
for task in tasks
    append!(result , fetch(task.task) )
end
jldsave("experiments/alt-iteration.jld2"; result)

```

```

using JLD2
using DataFrames
using ProgressMeter
using Random
<<init>>
<<setup-diverse-testgrids>>

#tests = [testgrid(relaxed_multi_solver, M , 2;alpha=82000 , epsilon=0.009) for M
#→ in initial_data]
tests = [testgrid(relaxed_multi_solver, M , 2 , h0=1.5e-3) for M in initial_data]

n = 64

```

## 12 Appendix

```
m = 1024

function iter(g::Vector{relaxed_multi_solver} , experiment , prg::Progress)
    out = []
    for j in 1:n
        set_xi_and_psi!(g[1])
        for i = 1:m
            elyps_solver!(g[1] , 100)
            SMOOTH!(g[1] , 1 ,true)
            next!(prg)
        end
        push!(out, (solver=deepcopy(g[1]), iteration=j , experiment=experiment))
    end
    return out
end

prg=Progress(size(tests ,1)*n*m , showspeed=true , )
tasks = []
for i in eachindex(tests)
    t = Threads.@spawn iter(tests[i], i , prg)
    push!(tasks , (iteration = 1 , task = t))
end
result = DataFrame()
for task in tasks
    append!(result , fetch(task.task) )
end
jldsave("experiments/test-nomulti-iteration.jld2"; result)
```

### 12.3.2 SUBITERATION

```
using DataFrames
using JLD2
using ProgressMeter
include(pwd() * "/src/solvers.jl")
include(pwd() * "/src/adapted_solvers.jl")
include(pwd() * "/src/utils.jl")
include(pwd() * "/src/multisolver.jl")
include(pwd() * "/src/multi_relaxed.jl")
include(pwd() * "/src/testgrids.jl")
include(pwd() * "/src/elypssolver.jl")
using Plots
using LaTeXStrings
using LinearAlgebra
```

```

using Printf
using ProgressBars
default(fontfamily="computer modern" , titlefontsize=32 , guifontsize=22 ,
    tickfontsize = 22 , legendfontsize=22)
pgfplotsx()
layout2x2 = grid(2,2)
layout3x1 = @layout [ b  c ; a]
size3x1 = (1600,1600)
SIZE = 64
M = testdata(SIZE, SIZE ÷ 5, SIZE /5 , 2)

incirc(M) = filter(x -> norm(x.I .- (size(M, 1) / 2, size(M, 2) / 2)) <
    min(size(M)... ) / 3, CartesianIndices(M))
insquare(M) = filter(x -> norm(x.I .- (size(M, 1) / 2, size(M, 2) / 2), Inf) <
    min(size(M)... ) / 4, CartesianIndices(M))
side(M) = filter(x -> x.I[2] < size(M, 2) ÷ 2, CartesianIndices(M))
halfcirc(M) = filter(x -> norm(x.I .- (1, size(M, 2) / 2), 2) < min(size(M)... ) /
    3, CartesianIndices(M))

function get_special_input(fn, size)
    M = fill(-1, size , size )
    M[fn(M)] .= 1
    return M
end
SIZE =64
t1= [testdata(SIZE, SIZE ÷ 5, SIZE /5 , j) for j in [1,2, Inf]]
t2 = [get_special_input(fn,SIZE) for fn in [halfcirc , incirc, side , insquare]]
initial_data = [t1 ; t2]
tests = [testgrid(multi_solver, M , 2) for M in initial_data]

#tests = [testgrid(relaxed_multi_solver, M , 2;alpha=32428.2 , epsilon=0.163398)
#    for M in initial_data]
tests = [testgrid(relaxed_multi_solver, M , 2) for M in initial_data]
n = 4
m = 1024

function iter(g::Vector{T} , n ,experiment , prg::Progress) where T<: solver
    out = []
    for j in 1:n
        set_xi_and_psi!(g[1])
        for i = 1:m
            elyps_solver!(g[1] , 1000
            alt_v_cycle!(g, 1)

```

## 12 Appendix

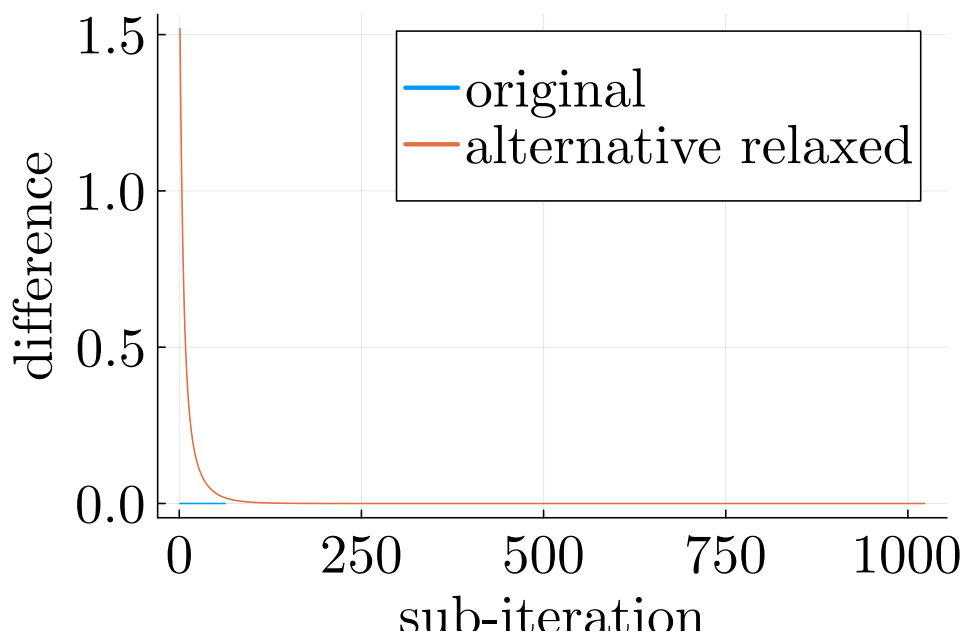
```
push!(out, (cycle=deepcopy(g[1]), iteration=j, subiteration=i,
            ↵ experiment=experiment))
next!(prg)
end
end
return out
end

tasks = []
prg=Progress(size(tests ,1)*n*m , showspeed=true , )
for i in eachindex(tests)
    t = Threads.@spawn iter(tests[i] , n , i , prg)
    push!(tasks , (iteration = 1 , task = t))
    end
result = DataFrame()
for task in tasks
    append!(result , fetch(task.task) )
    end
jldsave("experiments/alt-relaxed-subiteration.jld2"; result)
```

## 12.4 ALTERNATIVE RESULTS

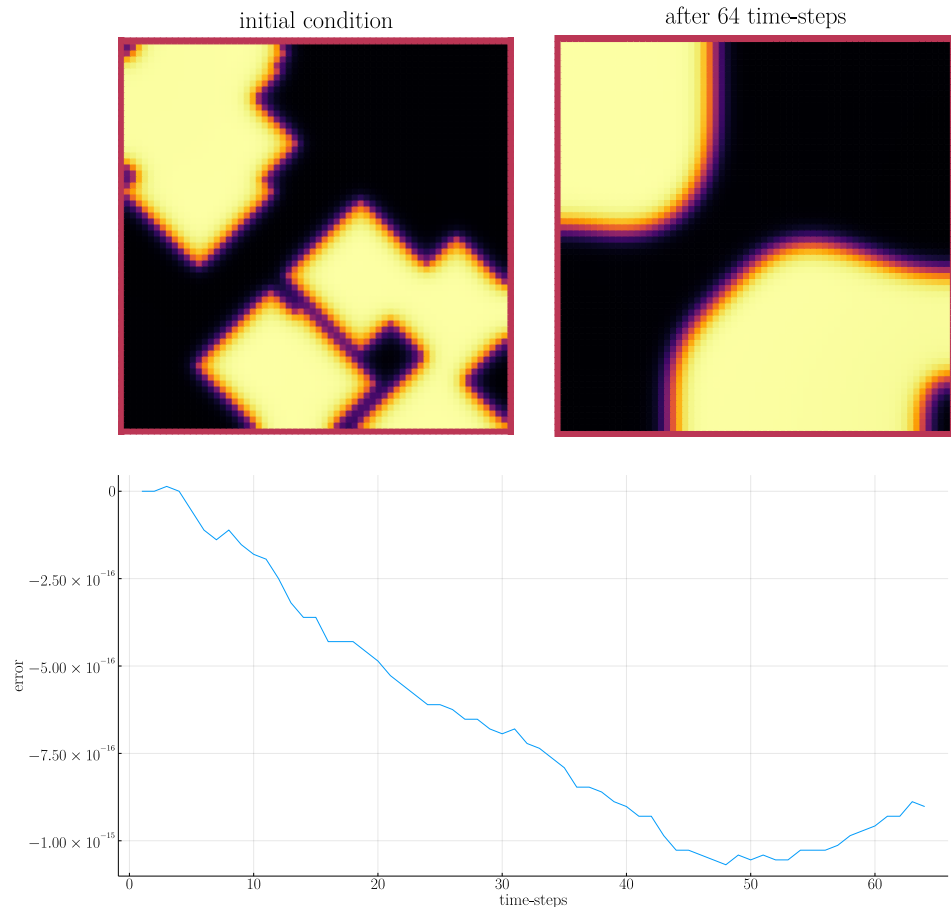
### 12.4.1 ITERATION

### 12.4.2 SUBITERATION



### 12.4.3 MASS

## 12 Appendix



### 12.5 MONTE CARLO OPTIMIZER

```
using Distributions
using DataFrames
using JLD2
include(pwd() * "/src/solvers.jl")
include(pwd() * "/src/adapted_solvers.jl")
include(pwd() * "/src/utils.jl")
include(pwd() * "/src/multisolver.jl")
include(pwd() * "/src/multi_relaxed.jl")
include(pwd() * "/src/testgrids.jl")
include(pwd() * "/src/elypssolver.jl")
using Plots
using LaTeXStrings
using LinearAlgebra
using Printf
```

```

using ProgressBars
default(fontfamily="computer modern" , titlefontsize=32 , guifontsize=22 ,
↪ tickfontsize = 22 , legendfontsize=22)
pgfplotsx()
layout2x2 = grid(2,2)
layout3x1 = @layout [ b  c ; a]
size3x1 = (1600,1600)
SIZE = 64
M = testdata(SIZE, SIZE ÷ 5, SIZE /5 , 2)

function test_values(alpha_distribution::Distribution ,
↪ epsilon_distribution::Distribution , M)
    alpha = rand(alpha_distribution)
    eps = max(rand(epsilon_distribution) , 1e-10)
    relaxed_solver = testgrid(relaxed_multi_solver, M, 2; alpha=alpha,
    ↪ epsilon=eps)
    set_xi_and_psi!(relaxed_solver[1])
    #SMOOTH!(relaxed_solver[1], 100, false)
    for j=1:64
        elyps_solver!(relaxed_solver[1], 2000)
        alt_v_cycle!(relaxed_solver , 1)
    end
    error = norm(relaxed_solver[1].phase .- original_solver[1].phase) /
    ↪ *(size(relaxed_solver[1].phase)...)
    return (;alpha=alpha , epsilon=eps , error=error)
end

original_solver = testgrid(multi_solver, M, 2)
set_xi_and_psi!(original_solver[1])
for j=1:64
    alt_v_cycle!(original_solver , 1)
end
#SMOOTH!(original_solver[1], 100, false);
eps = 3e-3
#M = testdata(64, div(64,3), 64/5 , 2)
alpha0 = 10000
epsilon0 = 1e-2
best_alpha = alpha0 / 10
best_epsilon = epsilon0 / 10
best_error = Inf
results = DataFrame()
for n=1:1000
    searchradius = 1

```

## 12 Appendix

```
alpha_distribution = Normal(best_alpha , searchradius * alpha0)
epsilon_distribution = Normal(best_epsilon , searchradius * epsilon0)
result = test_values(alpha_distribution , epsilon_distribution , M)
if result.error < best_error
    global best_error = result.error
    global best_alpha = result.alpha
    global best_epsilon = result.epsilon
    println(result)
end
push!(results , result)
end
jldsave("experiments/alpha-epsilon.jld2"; result=results)
println("Best alpha: $best_alpha , Best epsilon: $best_epsilon")
```

## 12.6 BULK ENERGY AND MASS BALANCE

```
function bulk_energy(solver::T) where T <: Union{multi_solver ,
→ relaxed_multi_solver}
    energy = 0
    dx = CartesianIndex(1,0)
    dy = CartesianIndex(0,1)
    W(x) = 1/4 * (1-x^2)^2
    for I in CartesianIndices(solver.phase)[2:end-1,2:end-1]
        i,j = I.I
        energy += solver.epsilon^2 / 2 * G(i+ 0.5,j ,solver.len, solver.width) *
        → (solver.phase[I+dx] - solver.phase[I])^2 + G(i,j+0.5,solver.len
        → ,solver.width) * (solver.phase[I+dy] - solver.phase[I])^2 +
        → W(solver.phase[I])
    end
    return energy
end

function massbal(arr)
    num_cells= *((size(arr).-2)...)
    return sum(arr[2:end-1, 2:end-1])/num_cells
end
```

## BIBLIOGRAPHY

- [1] Jaemin Shin, Darae Jeong, and Junseok Kim. “A conservative numerical method for the Cahn–Hilliard equation in complex domains”. In: *Journal of Computational Physics* 230.19 (2011), pp. 7441–7455. ISSN: 0021-9991. DOI: <https://doi.org/10.1016/j.jcp.2011.06.009>. URL: <https://www.sciencedirect.com/science/article/pii/S0021999111003585>.
- [2] Hao Wu. “A review on the Cahn–Hilliard equation: classical results and recent advances in dynamic boundary conditions”. In: *Electronic Research Archive* 30.8 (2022), pp. 2788–2832. DOI: [10.3934/era.2022143](https://doi.org/10.3934/era.2022143). URL: <https://doi.org/10.3934%2Fera.2022143>.